Supplementary Information: Mechanism of O_2 diffusion and reduction in [FeFe] hydrogenases

Adam Kubas,[†,‡,@] Christophe Orain,[¶,@] David De Sancho,[§,@] Laure Saujet,[‖] Matteo Sensi,[¶] Charles Gauquelin,[⊥] Isabelle Meynial-Salles,[⊥] Philippe Soucaille,[⊥] Hervé Bottin,[‖] Carole Baffert,[¶] Vincent Fourmond,[¶] Robert B. Best,[#] Jochen Blumberger,[*,†] and Christophe Léger[*,¶]

E-mail: j.blumberger@ucl.ac.uk; christophe.leger@imm.cnrs.fr

[*]To whom correspondence should be addressed

[†]Department of Physics and Astronomy, University College London, Gower Street, London WC1E 6BT, UK

[‡]Institute of Physical Chemistry, Polish Academy of Science, ul. Kasprzaka 44/52, Warsaw, Poland

[¶]Aix Marseille Université, CNRS, BIP UMR 7281, 13402, Marseille, France.

[§]Department of Chemistry, University of Cambridge, Lensfield Road, Cambridge CB2 1EW, United Kingdom; CIC nanoGUNE, Tolosa Hiribidea 76, 20018 Donostia-San Sebastián, Spain and IKERBASQUE; Basque Foundation for Science, María Díaz de Haro 3, 48013 Bilbao, Spain

[‖]Institut de Biologie et de Technologies de Saclay IBITECS, SB2SM, F-91191 Gif sur Yvette, France / Institut de Biologie Intégrative de la Cellule I2BC, UMR 9198, CEA, CNRS, Université Paris Sud, F-91191 Gif sur Yvette, France

[⊥]Université de Toulouse, INSA, UPS, INP, LISBP, INRA:UMR792,135 CNRS:UMR 5504, avenue de Rangueil, 31077 Toulouse, France

[#]Laboratory of Chemical Physics, National Institute of Diabetes and Digestive and Kidney Diseases, National Institutes of Health, Bethesda, Maryland 20892-0520, United States

[@]Contributed equally to this work.

Contents

S1 Derivation of expression for k_i, Eq. 3 in main text.

The inhibition of FeFe-hydrogenase with O_2 is described by the bimolecular rate constant k_i and the reverse process by the unimolecular rate constant k_a.

$$[\mathbf{FeFe}]\,(\mathrm{A}) \underset{k_a}{\overset{k_i[\mathrm{O_2}]}{\rightleftharpoons}} [\mathbf{FeFe}]-\mathbf{O_2}\,(\mathrm{I}) \tag{S1}$$

The inhibition is further divided in a diffusion process with rate constants k_{+1} and k_{-1} and chemical attachment/detachment with rate constants k_{+2} and k_{-2}.

$$[\mathbf{FeFe}]\,(\mathrm{A}) \underset{k_{-1}}{\overset{k_{+1}[\mathrm{O_2}]}{\rightleftharpoons}} [\mathbf{FeFe}]...\mathrm{O_2}\,(\mathrm{G}) \underset{k_{-2}}{\overset{k_{+2}}{\rightleftharpoons}} [\mathbf{FeFe}]-\mathbf{O_2}\,(\mathrm{I}) \tag{S2}$$

The time dependence of the concentrations of the geminate state G, inhibited state I and active state A are given by the usual kinetic equations,

$$\frac{\mathrm{d}[\mathrm{G}]}{\mathrm{d}t} = k_{+1}[\mathrm{A}][\mathrm{O_2}] + k_{-2}[\mathrm{I}] - (k_{-1}+k_{+2})[\mathrm{G}] \tag{S3}$$

$$\frac{\mathrm{d}[\mathrm{I}]}{\mathrm{d}t} = k_i[\mathrm{A}][\mathrm{O_2}] - k_a[\mathrm{I}] = k_{+2}[\mathrm{G}] - k_{-2}[\mathrm{I}] \tag{S4}$$

$$\frac{\mathrm{d}[\mathrm{A}]}{\mathrm{d}t} = k_a[\mathrm{I}] - k_i[\mathrm{A}][\mathrm{O_2}] = k_{-1}[\mathrm{G}] - k_{+1}[\mathrm{A}][\mathrm{O_2}] \tag{S5}$$

At equilibrium, $\frac{\mathrm{d}[\mathrm{I}]}{\mathrm{d}t} = \frac{\mathrm{d}[\mathrm{A}]}{\mathrm{d}t} = \frac{\mathrm{d}[\mathrm{G}]}{\mathrm{d}t} = 0$ and $[\mathrm{A}] = [\mathrm{A}]_{\mathrm{eq}}$, $[\mathrm{I}] = [\mathrm{I}]_{\mathrm{eq}}$, $[\mathrm{G}] = [\mathrm{G}]_{\mathrm{eq}}$ and $[\mathrm{O_2}] = [\mathrm{O_2}]_{\mathrm{eq}}$. Insertion of these conditions in Eqs. S4 and S5 gives the equilibrium constants in terms of the rate

constants,

$$K_i \equiv \frac{[\mathrm{I}]_{\mathrm{eq}}}{[\mathrm{A}]_{\mathrm{eq}}[\mathrm{O_2}]_{\mathrm{eq}}} = \frac{k_i}{k_a} \tag{S6}$$

$$K_{+1} \equiv \frac{[\mathrm{G}]_{\mathrm{eq}}}{[\mathrm{A}]_{\mathrm{eq}}[\mathrm{O_2}]_{\mathrm{eq}}} = \frac{k_{+1}}{k_{-1}} \tag{S7}$$

$$K_{+2} \equiv \frac{[\mathrm{I}]_{\mathrm{eq}}}{[\mathrm{G}]_{\mathrm{eq}}} = \frac{k_{+2}}{k_{-2}}. \tag{S8}$$

Therefore, $K_i = K_{+1}K_{+2}$ and

$$k_a = \frac{k_{-1}k_{-2}}{k_{+1}k_{+2}}k_i. \tag{S9}$$

To describe the kinetics of reaction schemes such as the one shown in Eq. S2, one usually assumes the steady-state approximation for the intermediate state, here state G. That is, after a short initial window of time, the concentration of G is assumed to remain unchanged during the course of the reaction,

$$\frac{\mathrm{d}[\mathrm{G}]}{\mathrm{d}t} = 0. \tag{S10}$$

In previous work on ligand diffusion in the enzyme CODH/ACS, the steady state assumption Eq. S10 was shown to give an excellent approximation.[1] Here, we make a second assumption, $k_{-2} \ll k_{+2}$, which is indeed valid for the reaction we consider in this work (see main text). Hence, at the beginning of the reaction where the concentration of I is still low, the reaction from I back to G can be neglected,

$$k_{-2}[\mathrm{I}] \ll \mathrm{k}_{+2}[\mathrm{G}], \tag{S11}$$

and therefore also the reaction from I back to A,

$$k_a[\mathrm{I}] \ll k_{+2}[\mathrm{G}]. \tag{S12}$$

Insertion of Eqs. S10 and S11 in Eq. S3 gives

$$[\mathrm{A}][\mathrm{O_2}] = \frac{k_{-1}+k_{+2}}{k_{+1}}[\mathrm{G}], \tag{S13}$$

and insertion of Eqs. S13, S11 and S12 in Eq. S4 gives the final expression for the inhibition rate,

$$k_i = \frac{k_{+1}}{k_{-1} + k_{+2}} k_{+2}. \tag{S14}$$

The rate for re-activation (here detachment and diffusion out of the protein) is obtained by inserting Eq. S14 in Eq. S9,

$$k_a = \frac{k_{-1}}{k_{-1} + k_{+2}} k_{-2}. \tag{S15}$$

S2 MD simulation and Markov state model

In order to understand the dynamics of the diffusion of gas molecules from the solvent into the protein active site, we used an approach that has been developed previously by some of us.[1–5] The first step involves extensive atomistic molecular dynamics simulation of the protein and the gas molecules solvated in explicit water. The structure of *Clostridium acetobutylicum* (Ca) FeFe hydrogenase has not been resolved experimentally and the structure available for *Chlamydomonas reinhardtii* (Cr) FeFe hydrogenase does not include the mature H-cluster.[6] Hence we have resorted to use the structure of their homolog from *Clostridium pasteurianum* (Cp) to run the simulations (PDB id: 3c8y[7]). Although the details of the diffusion may change slightly from protein to protein, we note that there is good support for the transferability of the results. In the alignment between the three sequences we find that the identity between Cp and Ca is very high (71.5%; see also Fig. S2a). In the case of Cr, the sequence identity is considerably lower (34.5%). However the sequence similarity is high in the region corresponding to the main access paths (see Fig. S2b), and particularly for the residues that line the access tunnels we mostly find identity between the three sequences (see colour code in Fig. S1). To finalize we note that even the Cr structure lacking the mature H-cluster has very good structural similarity (1.89 Å *RMSD*) over the aligned region with the Cp enzyme used in the simulations (see Fig. S2c).

As detailed below we have run a combination of long equilibrium simulations where we aimed for broad sampling of ligand diffusion within the protein and the solvent, and shorter runs from

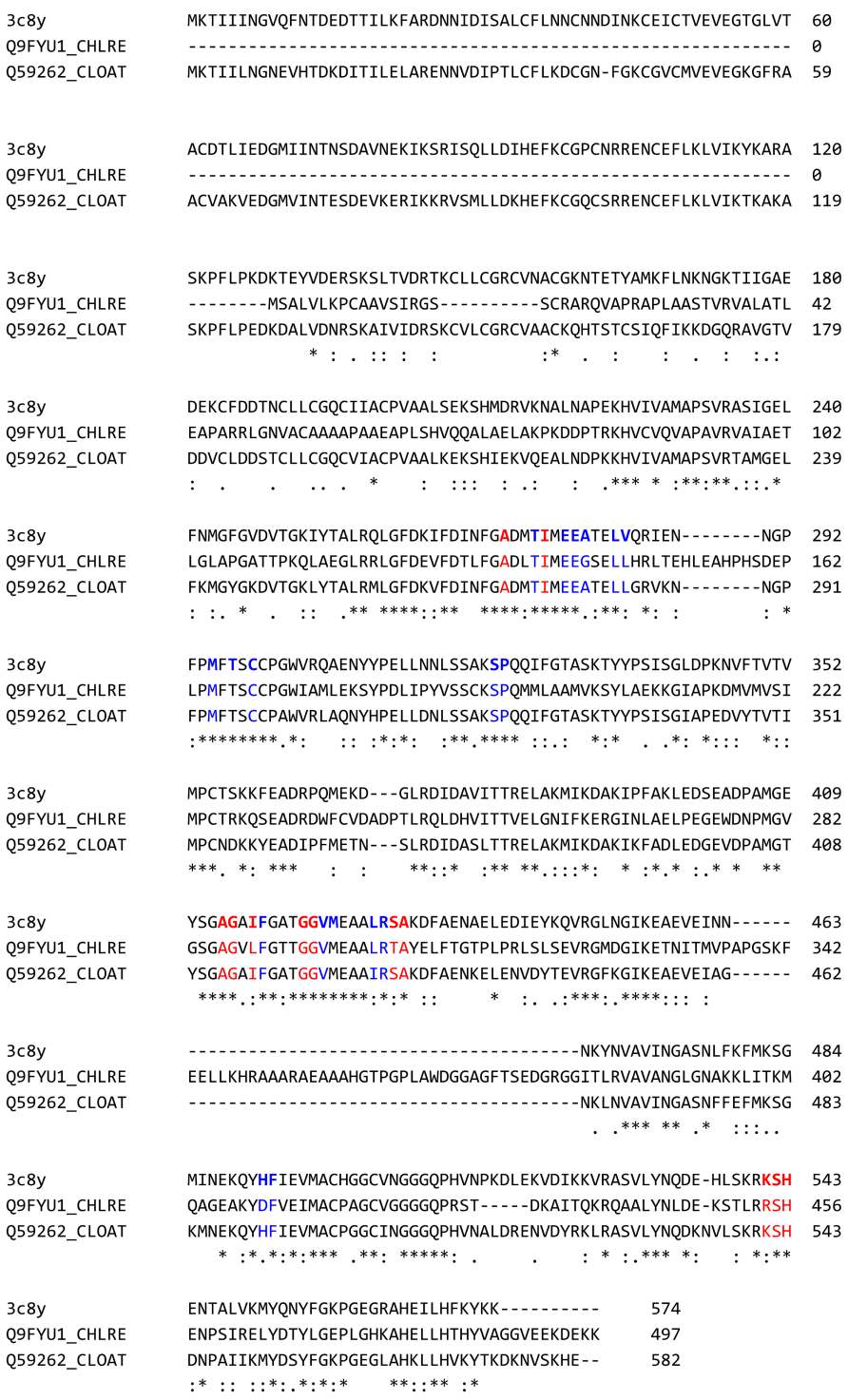

Figure S1: Alignment of the Cp (PDB: 3C8Y), Ca (Uniprot: Q9FYU1) and Cr (Uniprot: Q59262) FeFe hydrogenase sequences produced using the Clustal[8] implementation included in the MultiSeq extension[9] of the VMD program.[10] Residues coloured in blue and red are lining the main access paths (1 and 2, respectively) to the H-cluster.

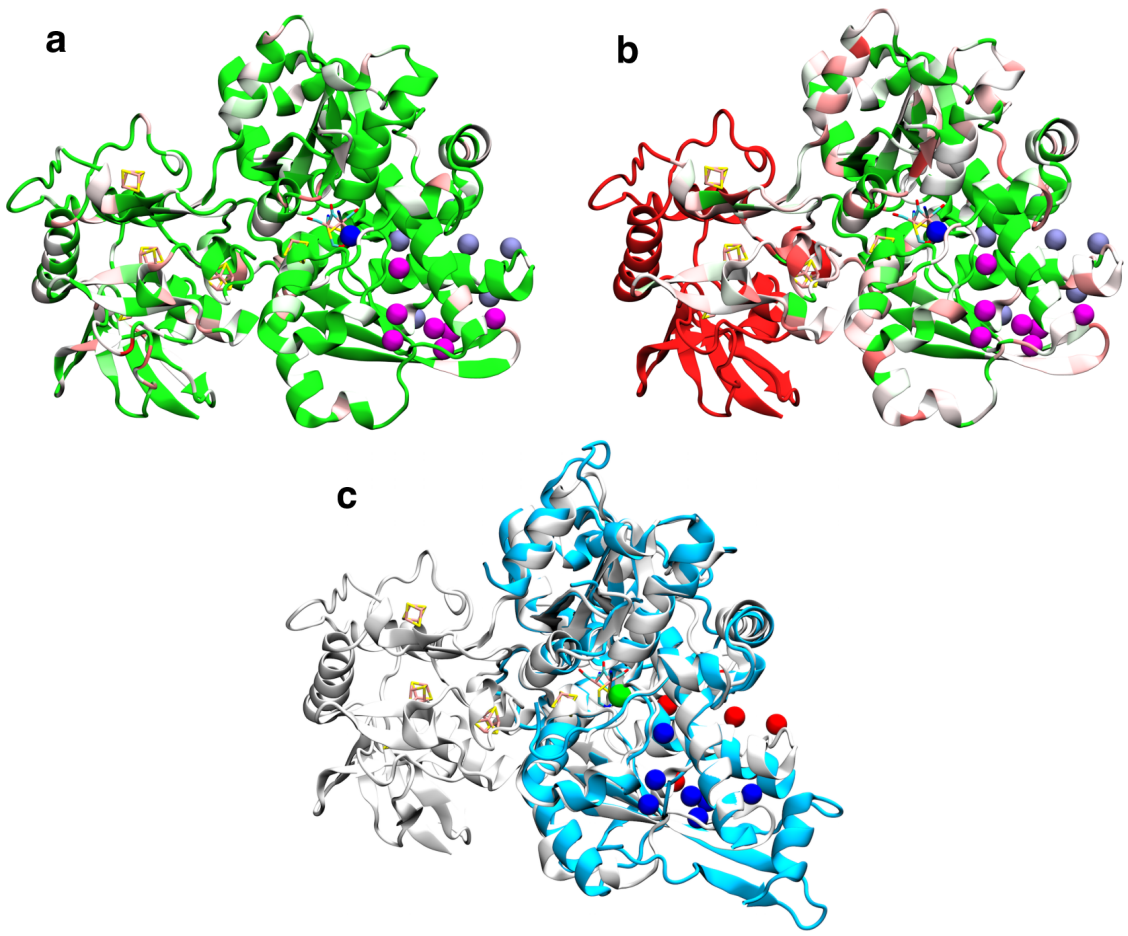

Figure S2: (a-b) Cartoon representation of Cp hydrogenase with atomic detail for metal clusters and magenta and ice blue spheres indicating the clusters involved in the main access paths reaching the geminate site (blue sphere). The red-white-green colour code indicates structure similarity between Cp and Ca (a) and Cp and Cr (b), with red indicating low similarity and green indicating high similarity. The BLOSUM80 similarity scoring matrix was used. (c) Overlay between the experimental structure of immature Cr (cyan) and Cp (white). Color code of relevant clusters as in the main manuscript. Figures were produced using the MultiSeq extension[9] of the VMD program.[10]

the pockets deep inside the protein to improve the statistics, resulting in an aggregate simulation time of over 1.9 μs. All simulations were carried out using the Gromacs software package, version 4.6.[11]

S2.1 Force field parameters

We used the optimized Amber03w force field[12] together with the TIP4P/2005 water model.[13] Parameters for the active site cluster and iron-sulfur clusters were taken from the DFT-derived force field of Chang and Kim.[14] For the O_2 molecule we used a three-site model, with a bond length between the O_2 atoms of 1.21 Å and a mass-less virtual site located in the center of mass of the gas molecule. The oxygen atoms carry charges of -0.114 and the virtual atom 0.228, in order to reproduce a quadrupole moment.[15,16] The Lennard-Jones parameters for the virtual atom are $\varepsilon = 0.4305$ kJ/mol and 3.01 Å.

S2.2 Equilibrium MD

First, we run two sets of long ($\sim$100 ns) equilibrium simulations of the protein together with 50 O_2 molecules. The initial structure was energy minimized using a conjugate gradient algorithm. Then the protein molecule was solvated in a truncated octahedron water box with 79.2 Å between closest walls, including 29807 water molecules, and then further energy minimized. Water molecules were replaced to include 75 Na^+ and 60 Cl^- ions to the simulation box. The resulting simulation system was used as the starting point for a short NVT simulation at 300 K with position restraints in the protein and metal clusters. Finally long equilibrium simulations were run at 300 K using a stochastic leap frog integrator with an integration timestep of 2 fs and a friction coefficient of 1 ps^{-1}. The particle-mesh Ewald method was used for the electrostatics[17] with a grid spacing of 1.2 Å and a real-space cutoff of 9 Å.

In the long equilibrium runs none of the 50 gas molecules reached the proximity of the H-cluster. In the spirit of adaptive sampling[18] we initialized tens of short simulations from the closest sites to the active site, and from the active site itself. Even this was insufficient for sampling the last transitions from the protein pockets to the active site. A summary of the actual runs and total simulation time is shown in Table S1.

Table S1: Summary of the equilibrium atomistic molecular dynamics simulations run for this study.

Run	Number of runs	Simulation time [ns]	Aggregate time [ns]
Equilibrium 1	1	92.6	92.6
Equilibrium 2	1	142.4	142.4
Short Eq. 1	5	20	100
Short Eq. 2	5	20	100
Short Eq. 3	5	20	100
Short Eq. 4	5	20	100
Short Eq. 5	5	20	100
Short Eq. 6	5	20	100
Short Eq. 7	5	20	100
Short Eq. 8	50	20	1000
Total	87		1935

S2.3 Pulling simulations

For a subset of the microstates from the model (those closest to the H-cluster), we have run simulations in the presence of an external pulling force. To set up these runs, we first placed a single O_2 molecule at the center of a cluster corresponding to a microstate using a randomly chosen snapshot of the solvated protein. The resulting system was energy minimized and a short NVT simulation in the presence of position restraints was run to avoid very high forces. Then short simulations in the presence of an external pulling force were run using the pull code from the Gromacs software package.[11] The center of mass of the gas molecule was dragged towards a reference site, defined as the center of mass of a selection of atoms from the H-cluster, shown in Figure S3.

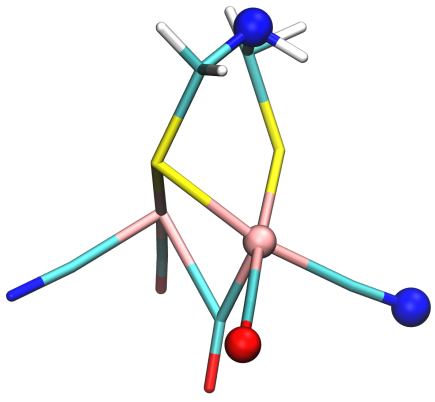

Figure S3: Representation of the H-cluster, with selected atoms used as target site for the pulling simulations represented as spheres.

S2.4 Kinetics of barrier crossing processes induced by force

The results of the MD simulations of force induced transitions to the H-cluster were fitted using the Dudko-Hummer-Szabo model.[19] Briefly, this model assumes that the transitions in the presence of an external force can be explained as a diffusive barrier crossing process on a simplified free energy surface. The escape rate over the barrier is expressed as

$$k(F) = k_0 \left(1 - \frac{\nu F x^{\ddagger}}{\Delta G^{\ddagger}}\right)^{1/\nu - 1} e^{(\Delta G^{\ddagger}[1-(1-\nu F x^{\ddagger}/\Delta G^{\ddagger})^{1/\nu}])}, \tag{S16}$$

where the model parameters are the transition rate in the absence of force (k_0), the position of the transition state ($x^{\ddagger}$) and the free energy barrier ($\Delta G^{\ddagger}$). Another model parameter is ν, which determines the shape of the one-dimensional potential (in this case we set $\nu = 1/2$, corresponding to a linear cubic surface).[19]

For each of the pulling simulations i at force F, we calculate the transition time t_i as the time it takes for the distance to reach the H-cluster site (we set the cutoff distance for an effective transition at 2.5 Å from the selected atoms of the H-cluster, corresponding to the center of the distribution of gas molecules in that site; see Figure S4). To calculate the maximum likelihood transition time for the N runs started from each microstate we use the expression

$$\tau = N_b^{-1} \{ \sum_{i=1}^{N_b} t_i + \sum_{i=N_b+1}^{N} T_i \}, \tag{S17}$$

where T_i is the total time of the simulations that did not reach the H-cluster and N_b is the total number of trajectories that bind. Errors were estimated as $\tau / N_b^{1/2}$.

In Figure S5 we show the results from the pulling simulations for those sites from which we observe that binding is most likely. The theory for force-induced transitions explains the data very well, and returns values for the rate in the absence of force, k_0, which we later combine with the rates derived from the Markov state model.

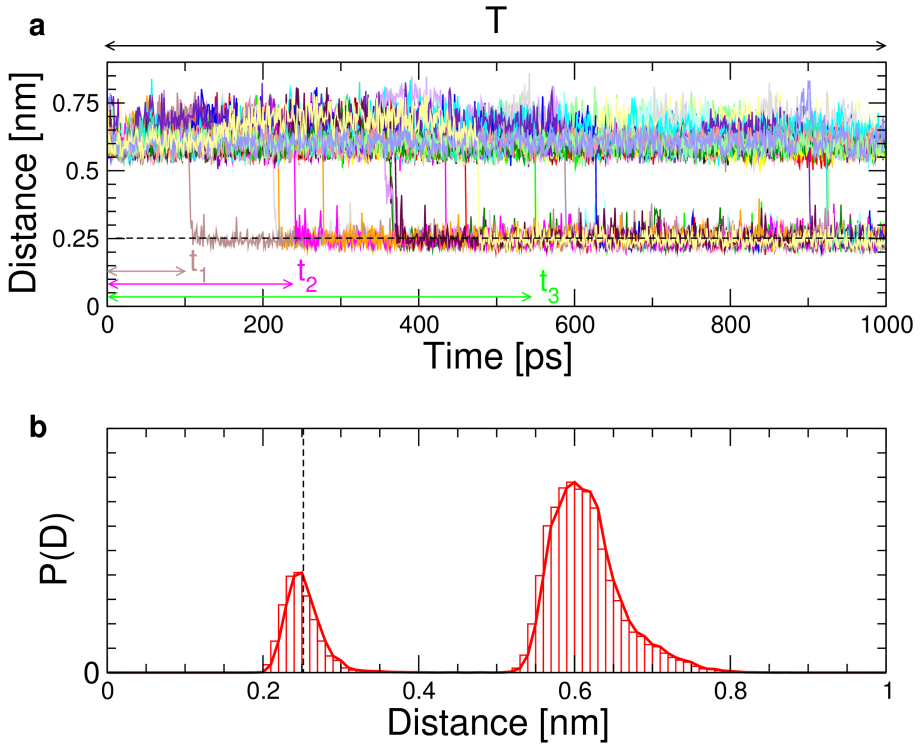

Figure S4: (a) Time series for the distance between the virtual atom of the O_2 molecule and the center of mass of the selected atoms from the H-cluster, calculated from 50 MD pulling runs. We mark illustrative examples of transition times t_i for three runs as well as the total simulation length T. (b) Distribution of values of the distance calculated for the same dataset. In both plots the dashed line marks the distance at which we assume that the geminate site has been reached.

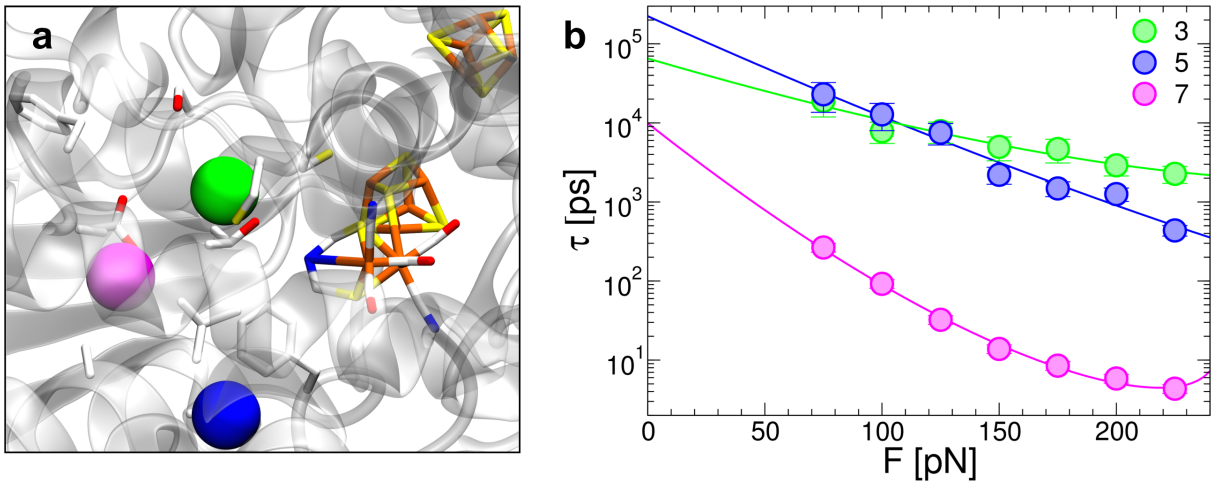

Figure S5: (a) Selected initial states for the pulling simulations (spheres). Atomic detail is shown also for the H-cluster. The protein is shown as transparent ribbon. (b) Force dependent binding times estimated from simulations initiated from the different initial states (colours as in (a)). Fits to the Dudko-Hummer-Szabo theory are shown as lines.

S2.5 Markov state model of gas diffusion in hydrogenase

We describe the kinetics of gas diffusion of the O_2 molecules within the protein using a Markov state model (MSM).[20–22] The MSM was built using the methods described previously.[5] We briefly summarize the methodology below. The construction of an MSM involves the following steps: discretizing the MD simulation data, assigning the transitions to the microstates, estimating the transition count and rate matrices, and validating the model.

Discretization. The coordinates of the O_2 molecules from the long equilibrium runs within a maximum of 6 Å from protein heavy atoms were clustered using the Daura algorithm with a cutoff of 5 Å.[23] We filtered the initial set of clusters, including only the most populated clusters which account for up to a 95% of the total simulation time. This resulted in a total of 212 microstates.

Assignment. For assigning an instantaneous position of an O_2 molecule to one of the clusters we used transition based assignment (TBA).[22,24] For each of the clusters, we calculated the distribution of distances from each of the cluster members to the cluster center, and defined a TBA radius, r_{TBA}, as the value corresponding to the distance that lies at the median of the population of the cluster. Each of the O_2 atoms from each instantaneous configuration was then assigned to a microstate i whenever the virtual atom of the O_2 was closer than $r_{\mathrm{TBA}}(i)$ from the corresponding cluster center. A transition from a microstate i to another microstate j was assigned only if after leaving microstate i, the virtual site of the gas molecule approached the center of cluster j at less than $r_{\mathrm{TBA}}(j)$. This type of assignment greatly reduces the number of recrossings, which would result in artificially fast rates.[22] For escaping from any of the microstates to the solvent, we imposed a hard cutoff distance of 6 Å from any alpha carbon of the protein. Using this criterion we assigned all trajectories to the model microstates.

Estimation of rate matrix. Using the assigned trajectories one can simply calculate the transition count matrix, $\mathbf{N}(\Delta t)$, with elements $N_{ji}(\Delta t)$ corresponding to the number of transitions observed from state i to state j within an observation window (or lag time) Δt. From the transition count matrix we obtain the transition probability matrix $\mathbf{T}(\Delta t)$, with elements calculated using the

maximum likelihood estimator[25]

$$t_{ji}(\Delta t) = N_{ji}(\Delta t) / \sum_j N_{ji}(\Delta t) \tag{S18}$$

To obtain the rate matrix $\mathbf{K}(\Delta t)$ we use the approximation $k_{ji}(\Delta t) = t_{ji}(\Delta t)/\Delta t$ for $i \neq j$ and $k_{ii}(\Delta t) = -\sum_j k_{ji}(\Delta t)$.[26] In Figure S6a we show the relaxation times from the rate matrix as obtained from the eigenvalues of the rate matrix $\tau_i = -1/\lambda_i$.

We connect the rate matrix calculated from the equilibrium MD runs to the fitted rates at zero force ($k_{Gi}(0)$) by adding a row and a column to the rate matrix (corresponding to the $G \rightarrow i$ and $i \rightarrow G$ transitions, respectively). The rates for the additional column are zero except for those microstates from which we run pulling simulations, for which we use $k_{Gi} = k_0$ from Equation S16. For the reverse rate (k_{iG}) we use the results from short equilibrium runs initialized in the H-cluster.

The rate coefficients k_{is} for the transitions from the solvent s to the microstates i in the protein as obtained by the above procedure depend on the gas concentration used in the MD simulation. In order to obtain the rate coefficients at a reference concentration $[O_2]^o$ =1 mM we scale the k_{is} by a factor of $V_{\text{sim}}^{H_2O}/V_{\text{ref}}^{o}$.[3] Here $V_{\text{sim}}^{H_2O}$ is the volume of water in the simulation, which we obtain from substracting the volume of the protein (V_{protein}=94.570 nm^3) from that of the simulation box

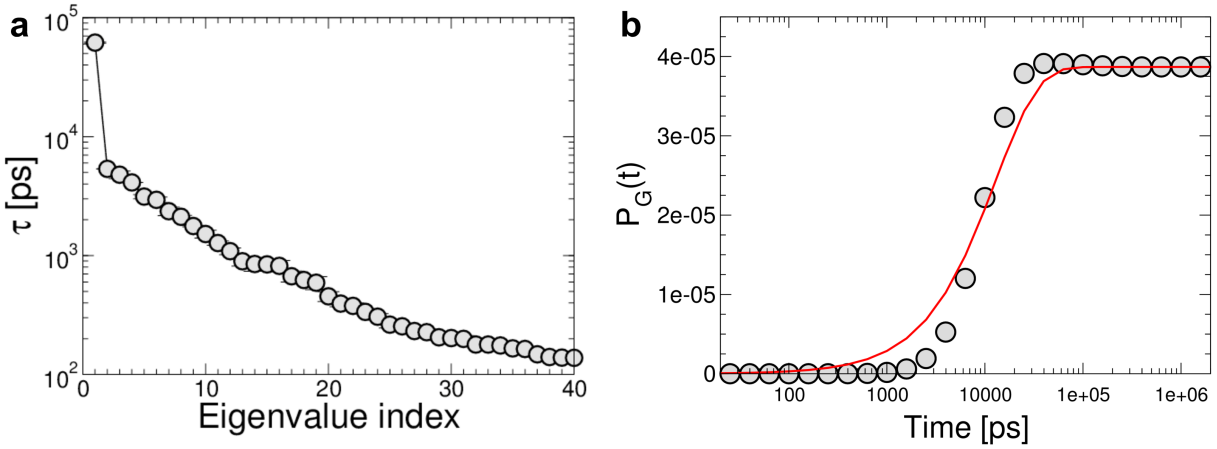

Figure S6: (**a**) Spectrum of eigenvalues of the rate matrix. Only the first 40 eigenvalues are shown. (**b**) Population of the geminate microstate as a function of time, from a calculated relaxation initiated in the solvent. The red line shows the fit to Equation S20

(V_{box}=993.588 nm^3). Then the simulated concentration of gas is [O_2]=1.847 mM and the scaling factor for the rate coefficients is $V_{sim}^{H_2O}/V_{ref}^{o}$=0.541.

Validation. The simplest test for the Markov property in an MSM is the convergence of relaxation times, τ_i as a function of the lag time. In Figure S7 we show that indeed relaxation times for the MSM are well converged and remain stable for a long range of lag times. The results reported in this paper correspond to a lag time of 1 ps.

Estimation of the binding rate from the MSM. We calculate the rate of access to the H-cluster as before,[2] using the propagation of the rate matrix from an initial distribution placed at the solvent microstate (hence $p_i(0) = 0$ for all states except $i = s$, where $p_s(0) = 1$). The relaxation can be calculated from the matrix exponential as

$$\mathbf{P}(t) = \exp(\mathbf{K}t)\mathbf{P}(0) \tag{S19}$$

In Figure S6b we show the relaxation for the geminate site $p_G(t)$. In order to obtain the rates of

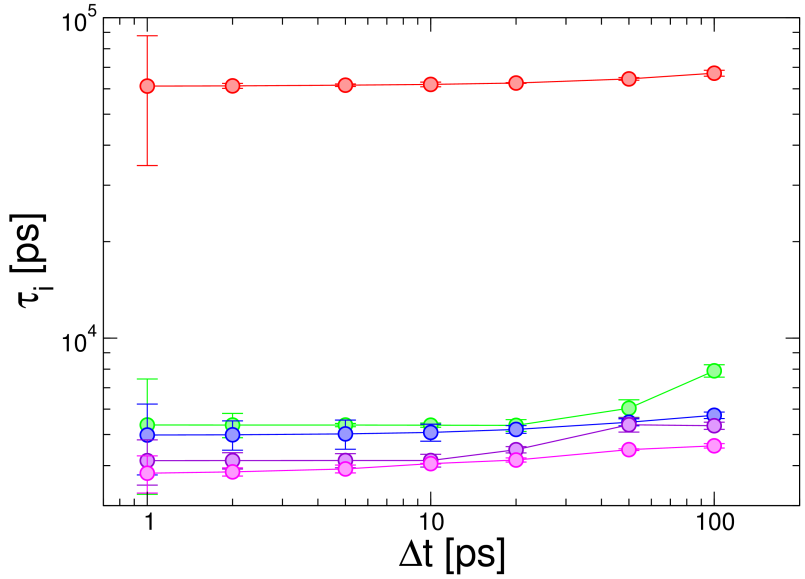

Figure S7: Convergence of relaxation times for the first few modes of the rate matrix. All times are in ps.

access to the geminate site we fit the data to the following expression

$$p_G(t) = \frac{k_{+1}[O_2]}{k_{+1}[O_2] + k_{-1}} [1 - \exp(-(k_{+1}[O_2] + k_{-1})t)] \tag{S20}$$

to obtain the values of k_{+1} and k_{-1}. The data is well explained by this pseudo-first order rate expression.

S2.6 Explicit simulations of mutants

For the F417W, F417Y and V423F we run explicit atomistic MD pulling simulations as described above, only for the last transition of the dominant pathway (i.e. for the 7→G step). The setup of these runs was done as described for the WT, with the initial structure corresponding to the highest ranked rotameric state, as defined by PyMOL. In the case of the V423F mutant simulations were run starting from the two most probable rotameric states. In Figure S8 we show the results. In all cases we obtain a slowdown of the final transition upon mutation. The effect is particularly strong for the mutations in site F417, where access to the geminate site via pathway 1 seems almost

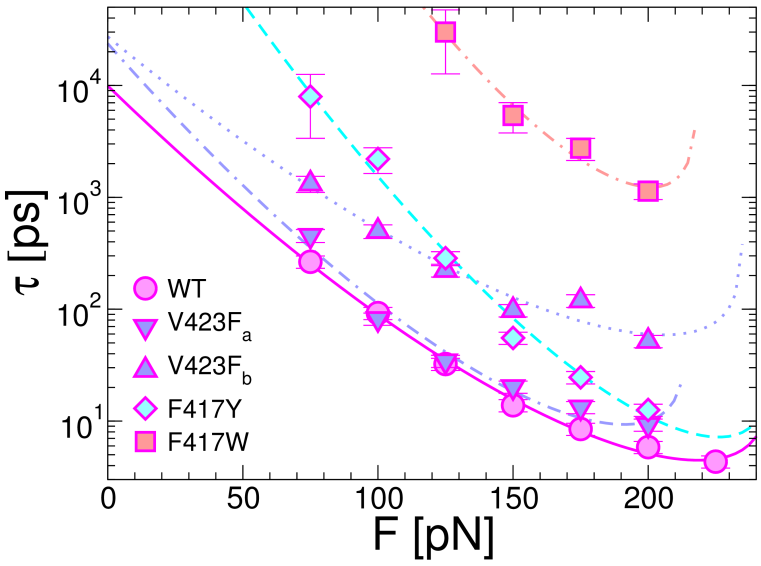

Figure S8: Force dependent binding times estimated from simulations initiated from site 7 for different mutants of Cp hydrogenase. Symbol filling colours correspond to different mutants. Lines, with the same colour code, are fits to the Dudko-Hummer-Szabo model.

completely inhibited. In the case of V423F we observe a slowdown for both rotameric states by a factor of about 2.

Table S2: Summary of the pulling simulations run for this study.

Pulling site	Pulling force [pN]	Number of runs	Simulation time [ns]
1	75	48	3
1	100	48	2
1	125	48	2
1	150	48	1
1	175	48	1
1	200	48	1
1	225	48	1
2	100	48	2
2	150	48	1
2	200	48	1
3	75	48	3
3	100	48	2
3	125	48	2
3	150	48	1
3	175	48	1
3	200	48	1
3	225	48	1
4	100	48	2
4	150	48	1
4	200	48	1
5	75	48	3
5	100	48	2
5	125	48	2
5	150	48	1
5	175	48	1
5	200	48	1
5	225	48	1
7	75	64	3
7	100	64	2
7	125	64	2
7	150	64	1
7	175	64	1
7	200	64	1
9	200	48	1
Total			2656

S3 Further discussion of the non-redox reactivation (k_a)

DFT structure optimizations of the O_2-bound state (structure **2** in Figure 5, main text) show that the O-O bond length increases from 1.22 Å to 1.30 Å upon binding and that the distal oxygen carries a negative charge, which is stabilized through hydrogen bonding with Cys169. The closest contact O-O^- $\cdots$ HS-Cys169 is 2.16 Å. Proton transfer (PT) from the sulphur to the distal oxygen is only slightly uphill by 2.2 kcal/mol and the PT activation barrier equates 7.5 kcal/mol. Hence, PT is orders of magnitude faster than reactivation, observed on the time scale of 10-100 seconds. Besides, the cysteine is part of the proton transfer chain that connects the active site to the solvent.[27–31] This, together with our calculations, suggests that a fast, solution pH-dependent protonation equilibrium between Fe_d-O_2 and Fe_d-O_2H^+ exists.

DFT calculations further show that dissociation of O_2H^+ from the active site is energetically unfeasible (104.8 kcal/mol), whereas dissociation of O_2 is slow but feasible with a free energy barrier of 20.0 kcal/mol.[32] In the alkaline limit, where O_2H^+ is negligible, and within the steady-state approximation for G, the re-activation rate for chemical detachment of O_2 and diffusion out of the protein is given by Eq. 15. Since $k_{-1} \gg k_{+2}$, $k_a = k_{-2} = 1.1 \cdot 10^{-2}\,\mathrm{s}^{-1}$. This compares favourably with the experimental estimate for the re-activation rate in the alkaline limit, $k_a > 1.0 \cdot 10^{-1}\,\mathrm{s}^{-1}$. The deviation between computation and experiment (at least a 9-fold underestimation of k_a) is similar to what we found for k_i (see main text). Here the deviation can only originate from chemical ligand detachment implying that the transition state of this step is indeed overestimated in the calculations of Ref. 32 by 1-2 kcal/mol.

S4 Quantum mechanical (QM) calculations

S4.1 Molecular model and electronic structure method

The energy and free energy for O_2 binding, reaction **1**$\rightarrow$**2** in Figure 5 main text, were taken from our previous study,[32] where calculations were carried out using a QM(CA1-B3LYP)/QM(BP86-

D3) ONIOM approach. The functional in the high-level QM region (CA1-B3LYP) was a range-separated functional, that was specially parametrized to reproduce the binding energy profile of high-level ab-initio calculations. Whereas short-range dispersion interactions for O_2 binding were described with that functional, the medium and long-range dispersion interaction of O_2 with protein residues were accounted for by BP86-D3. The binding free energy reported in Ref. 32, ΔG = -7.1 kcal/mol, was for O_2 initially residing in the G cavity, i.e. active site of the protein. We have modified this value so that the binding free energy corresponds to O_2 initially residing in the gas phase at standard conditions, O_2 (g). This gives a binding free energy ΔG = -2.7 kcal/mol, as indicated in Figure 5 in the main text.

The calculations on the species formed upon consecutive addition of electrons and protons, **3**-**9** in Figure 5 main text, and on the species described in SI section 3, were carried out in this work using the large active site model shown in Figure S9. It is similar to the one used for the O_2 binding reaction and was obtained from the crystal structure of the *Cp* protein. This model was found to be sufficiently large for all reactions investigated. For one reaction, the formation of the sulphenic acid **9** (SOH) from species **4**, we investigated a slightly modified model. The sulphenic acid is strongly stabilised by a hydrogen bond to the CN^- ligand, and we checked that this stabilization is not just an artifact of our model in which the cysteine residue is represented by a CH_3SH molecule with the carbon atom fixed to the crystal structure position. Inclusion of the entire cysteine (with C^α kept fixed to the crystal position) reduced only slightly the stabilisation of **9** relative to **4**, from 14 to 12 kcal/mol. Therefore our conclusion that **9** is an energetically low lying species remains unchanged.

We note that the N-atom of the bridging amino of the active site is thought to be involved in proton delivery to the active site. Therefore, under turnover conditions (H_2 production, no O_2 inhibition), this atom becomes temporarily doubly protonated. For our calculations we chose the singly protonated (neutral) state because our calculations indicated that proton transfer from the N-atom to bound O_2 is unlikely. The bound O_2 ligand is ideally positioned to accept a proton from Cys299, whereas proton transfer from the bridging N atom would require a major re-orientation

of O_2, which is energetically costly and highly unlikely to occur. Thus, whereas proton transfer from the amine is important under turnover conditions, we do not think it plays a major role for the initial stages of O_2 reduction. For this reason we treated the N-atom as singly protonated (neutral), as was done also in earlier work by Reiher et. al. (e.g. in 33 or 34).

The electronic structure of the active site model is complicated by the [Fe_4S_4] unit, which consists of two high-spin Fe(II) and two high-spin Fe(III) atoms that are antiferromagnetically coupled to yield a total spin of 0. This electronic state was approximated with the broken symmetry approach[35,36] using a coupling scheme as described previously.[32] Geometry optimisations were performed with the BP86 functional[37–41] augmented with empirical dispersion corrections using Becke and Johnson damping[42,43] (denoted by +D3 suffix). Def2-TZVP basis set was used throughout the study.[44,45] The calculations were performed efficiently with the resolution of the identity (RI) approximation[46,47] using the def2-TZVP/J auxiliary basis set.[48] Single point energies reported in the manuscript were obtained with the B3LYP+D3 functional[37,49,50] (see section S4.3 for validation of this functional) and COSMO solvation model[51] with either $\varepsilon = 4$ to account for the charge screening in a protein environment or $\varepsilon = 78$ in case of an aqueous solution. Geometry optimisations were carried out using the default DFT integration grid m3, whereas single point calculations utilised a larger grid m4. All DFT computations were performed with the Turbomole package[52] if not stated otherwise.

Each calculation was checked for the final spin populations to reassure convergence to the same broken-symmetry state. In Table S3 we summarize the natural spin population analysis (NPA)[53] for the four iron atoms of the cubane for each species **1**-**9** shown in Figure 5, main text, as obtained with the B3LYP functional plus COSMO solvation model. For each species we obtained very similar spin populations showing that the calculations have indeed converged to the same broken-symmetry state.

All structures were subjected to analytical frequency calculations to confirm they correspond to stationary points and to obtain harmonic corrections for ΔG. Because some atoms were fixed during optimisation, we obtained a few imaginary frequencies of small amplitude. They were ne-

Table S3: Natural spin population analysis for the four iron atoms of the cubane for each species **1**-**9** in Figure 5, main text, as obtained with B3LYP functional plus COSMO solvation model. The atom numbering is defined in Figure S9.

	Fe^1	Fe^2	Fe^3	Fe^4
1	3.457	3.449	-3.302	-3.319
2	3.445	3.441	-3.288	-3.327
3	3.457	3.433	-3.293	-3.328
4	3.427	3.451	-3.285	-3.324
5	3.480	3.430	-3.275	-3.327
6	3.386	3.358	-3.181	-3.217
7	3.385	3.463	-3.259	-3.296
8	3.457	3.449	-3.302	-3.319
9	3.437	3.457	-3.291	-3.319

glected in the calculation of thermochemical corrections. However, it was always verified that they do not involve any atoms important for the reaction studied. An alternative to omitting the imaginary frequencies is to remove from the Hessian all columns and rows that correspond to frozen atoms and calculate the free energy corrections from the eigenvalues of the modified Hessian. We have compared both methods for the two types of reactions considered in this work: (i) Reduction; we have chosen the reduction of the active site model [FeFe] (**1** in Figure 5, main text) as an example, $[FeFe]^0$ + 1 e^- $\rightarrow$ $[FeFe]^{1-}$. We obtained a total correction for the Gibbs free energy of ΔG_{corr}=-5.2 kcal/mol when omitting all imaginary frequencies and $\Delta G'_{corr}$=-6.2 kcal/mol when using the eigenvalues of the modified Hessian. (ii) Proton addition; we have chosen [FeFe]-O_2^{1-} + H^+ $\rightarrow$ [FeFe]OOH as an example. Here both approaches give virtually identical free energy corrections of -6.9 kcal/mol after rounding the first decimal digit. This suggests that the free energies reported are robust against the free energy correction scheme used. We think that this is mainly due to the fact that the same atoms are frozen in each consecutive step of the reaction and that the active site model is large enough so that the local changes at the di-iron site hardly affect the frequencies associated with frozen atoms.

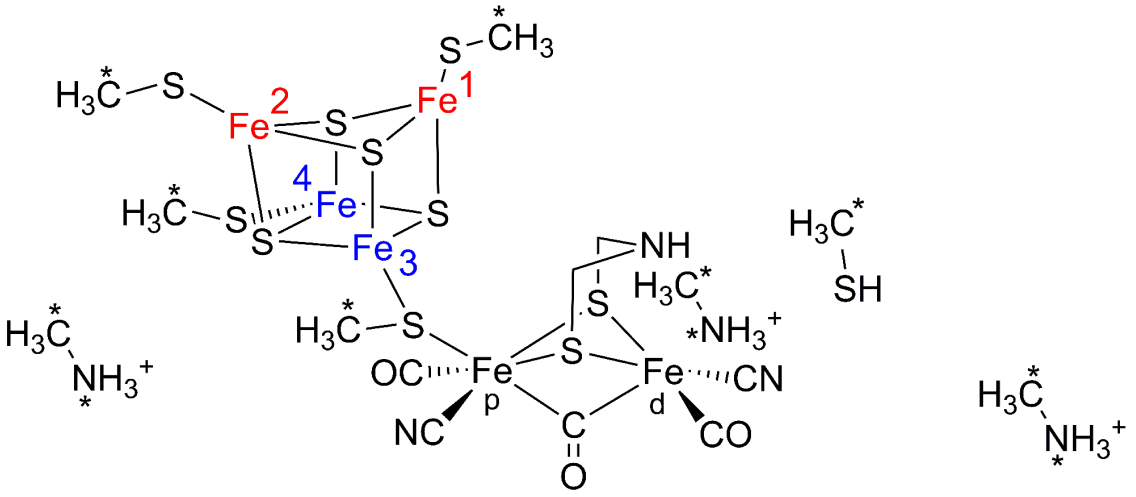

Figure S9: Scheme of the active site model used in this study. Atoms marked with asterisk were fixed to the crystal positions while the rest of the system was allowed to relax. The iron atoms 1 and 2 (red) as well as 3 and 4 (blue) are coupled ferromagnetically. The pairs (red-blue) are in turn coupled antiferromagnetically (see Table S3).

S4.2 Calculation of reaction free energies for PT coupled ET

There are three types of reactions in the reaction scheme of Figure 5, main text. The first reaction is binding of O_2 to the enzyme in state **1**

$$\mathbf{1} + O_{2(g)} \rightarrow \mathbf{2}, \tag{S21}$$

where (g) refers to the standard state in the gas phase and species **1** and **2** are in the solution phase at a standard activity of 1 mol/L. The electronic energies, zero-point energies, thermal corrections and entropic terms of **1** and **2** were calculated as explained in section S4.1 using the QM model of Figure S9 surrounded by a dielectric with ε=4. The properties for O_2 were calculated in the gas phase. The reaction energy difference (ΔE) and the free energy difference (ΔG) are summarized in Table S4. The difference between ΔE and ΔG, about 13 kcal/mol, is mainly due to the loss in translational entropy of the O_2 molecule.

The second type of reactions are the ET/PT steps. Calculations of absolute electron or proton attachment energies in the condensed phase are challenging because of the change in total charge and the resulting dependence of these energies on the absolute potential in the simulation cell. The

Table S4: Summary of computed reaction energies and free energies for the reactions shown in Figure 5 of main text. In $\mathbf{1} + O_2(g) \rightarrow \mathbf{2}$, O_2 (g) is at standard conditions. ET/PT steps are for pH=7 versus SHE.

	ΔE [kcal/mol]	ΔG [kcal/mol]
$\mathbf{1} + O_2(g) \rightarrow \mathbf{2}$	-16.1	-2.7
$\mathbf{2} + H^+(aq) + e^- \rightarrow \mathbf{3}$	-11.4	-6.2
$\mathbf{3} + H^+(aq) + e^- \rightarrow \mathbf{4}$	-33.4	-34.9
$\mathbf{3} + H^+(aq) + e^- \rightarrow \mathbf{5}$	5.8	8.6
$\mathbf{4} + H^+(aq) + e^- \rightarrow \mathbf{6}$	-4.9	0.7
$\mathbf{4} \rightarrow \mathbf{9}$	-16.9	-14.0
$\mathbf{6} + H^+(aq) + e^- \rightarrow \mathbf{7}$	-10.1	-12.9
$\mathbf{7} \rightarrow \mathbf{8}$	-7.8	-13.3
Total*	-82.7	-69.3

*O_2 + $4H^+$ + $4e^- \rightarrow 2H_2O$.
Exp. +1.23 V at pH = 0 vs. SHE.
This is -74 kcal/mol at pH =7 vs. SHE.

latter differs from the potential in experimental set-ups due to the presence of interfaces in experiment, use of electron core potentials and/or boundary conditions for potentials in the calculations. We avoided this complication by considering only coupled ET/PT steps so that the system remains neutral in all considered states. To ease the comparison with experimental data, all free energy differences for the ET/PT steps in Figure 5 in the main text were calculated for pH 7 and are relative to the free energy of the standard hydrogen electrode (SHE) reaction.

For example, considering the first ET/PT reaction in Figure 5,

$$\mathbf{2} + H^+_{(aq)} + e^- \rightarrow \mathbf{3}, \tag{S22}$$

and the SHE reaction,

$$H^+_{(aq)} + e^- \rightarrow \frac{1}{2} H_{2\,(g)}, \tag{S23}$$

the standard reaction free energy of reaction Eq. S22 relative to the SHE reaction Eq. S23 is equal

to the standard reaction free energy ΔG^0 of the hydrogenation reaction (Eq. S22 minus Eq. S23),

$$\mathbf{2} + \frac{1}{2}\mathrm{H_{2\,g}} \rightarrow \mathbf{3}. \tag{S24}$$

The electronic energy and free energy corrections for **2**, **3** and $\mathrm{H_{2\,(g)}}$ are calculated as described in section S4.1 to obtain ΔG^0. This way one obtains the standard reaction free energy of Eq. S22 vs SHE at a standard activity of $\mathrm{H^+_{(aq)}}$ of 1 mol/l, i.e. at pH = 0. To obtain the reaction free energy at pH=7 vs SHE, we add the usual concentration term $\ln 10\, k_\mathrm{B} T$ pH to ΔG^0, which amounts to an increase in ΔG^0 by 9.60 kcal/mol. Calculations are carried out similarly for the other ET/PT reactions shown in Figure 5.

The third type of reactions are unbinding events, e.g.

$$\mathbf{5} \rightarrow \mathbf{1} + \mathrm{H_2O_{2\,(aq)}}, \tag{S25}$$

$\mathrm{H_2O_{2\,aq}}$ is modelled as a cluster containing four explicit water molecules surrounded with a dielectric continuum. This gives a more accurate description of solvation than a pure dielectric continuum model. The reaction free energy reported corresponds then to the following reaction,

$$\mathbf{5} + (\mathrm{H_2O})_{4\,(aq)} \rightarrow \mathbf{1} + [\mathrm{H_2O_2(H_2O)_4}]_{(aq)}. \tag{S26}$$

The electronic energies and free energy corrections of the species in reaction Eq. S26 are calculated as explained in section S4.1. Calculations are carried out similarly for unbinding of OOH, OH and water.

S4.3 Validation of QM calculations

We have carried out extensive benchmark calculations to identify a density functional that would describe the oxygen reduction at the FeFe-hydrogenase active site with good accuracy. To this end we have carried out two series of calculations. Firstly, we chose a small test model of the

active site and calculated reaction energies for the first steps of oxygen reduction at the small active site model.The performance of several density functionals was compared to *ab initio* reference calculations at the level of the parametrized coupled cluster method with single and double excitations [pCCSD(-1,1)] using the def2-TZVP basis set (see Table S5). Secondly, we computed reduction and deprotonation free energies of oxygen species in aqueous solution and compared to experimental data (see Figure S10).

The small test model of the active site comprised of only the diiron subsite terminated with a CH_3SH group (for the details see Ref. 32). We tested various functionals (BP86, TPSS,[54] B3LYP, PBE0,[55,56] BHLYP,[37,38,40,50] CAM-B3LYP[57] along with corresponding D3 correction against pCCSD(-1,1).[58] The special parametrization accounts partially for missing higher-order excitations and improves the results substantially. The calculations would be prohibitively expensive without recently developed local pair natural orbital approach (LPNO)[59] that greatly reduces the virtual excitation space but provides results that are typically within ± 1 kcal/mol of the canonical calculations. We note, that particularly LPNO-pCCSD is both efficient and accurate method that approaches CCSD(T) accuracy at a fraction of cost.[60] The structures were optimised using setup described in the section S4.1. Calculations were performed with the Turbomole package, except the CAM-B3LYP and reference LPNO-pCCSD computations, which were carried out with the ORCA 3.0.3 program.[61] In case of the LPNO-pCCSD the T_1 diagnostic was found to be always between 0.022 and 0.026 in calculations involving the [2Fe] subunit and 0.014 for a free triplet oxygen molecule. The general agreement is that CC calculations that show $T_1 < 0.04$ can be considered as reliable.[62] The results are summarized in Table S5. We found that the B3LYP functional shows best overall performance with a mean unsigned error (MUE) of 2.31 kcal/mol and relative unsigned error (MRUE) of 8%, closely followed by the range-separated version of the same functional, CAM-B3LYP.

Table S5: Comparison of the electronic energy changes (kcal/mol) for eight reactions involving a small diiron model of [FeFe] hydrogenase active site adopted from 32. At the bottom of the table statistical evaluation of the density functionals with respect to the reference LPNO-pCCSD calculations is provided (MUE: mean unsigned error, MRUE: mean relative unsigned error, RMSD: root mean square deviation, MAX($\pm$): maximum singed positive or negative error). All calculations utilize the def2-TZVP basis set.

Reaction	BP86	TPSS	B3LYP	PBE0	BHLYP	CAM-B3LYP	LPNO-pCCSD
$[FeFe]^{1-} + 1e^- \rightarrow [FeFe]^{2-}$	11.60	16.95	22.74	26.34	45.49	25.12	21.55
$[FeFe]^{1-} - 1e^- \rightarrow [FeFe]^{0}$	75.30	72.03	75.51	77.57	74.33	73.03	74.19
$[FeFe]^{1-} + O_2 \rightarrow [FeFe] - O_2^{1-}$	-9.84	-11.47	-2.11	-0.58	10.36	-2.52	-1.93
$[FeFe]^{2-} + O_2 \rightarrow [FeFe] - O_2^{2-}$	4.41	3.06	15.01	18.96	13.69	7.57	11.62
$[FeFe] - O_2^{1-} + 1e^- \rightarrow [FeFe] - O_2^{2-}$	25.84	31.48	39.86	45.88	48.83	35.22	35.11
$[FeFe] - O_2^{1-} + H^+ \rightarrow [FeFe] - O_2H$	-309.20	-311.72	-311.51	-312.02	-316.93	-309.27	-315.00
$[FeFe] - O_2^{2-} + H^+ \rightarrow [FeFe] - O_2H^{1-}$	-415.17	-420.37	-429.99	-436.83	-445.21	-427.78	-431.46
$[FeFe] - O_2H + 1e^- \rightarrow [FeFe] - O_2H^{1-}$	-80.13	-77.16	-78.63	-78.93	-79.45	-83.28	-81.35
MUE [kcal/mol]	7.35	5.88	2.31	4.80	8.72	2.60	
MAX(+) [kcal/mol]	16.29	11.09	4.75	10.77	23.94	5.72	
MAX(-) [kcal/mol]	-9.96	-9.54	-0.18	-5.37	-13.75	-4.05	
RMSD [kcal/mol]	8.67	6.66	2.72	5.59	11.79	3.18	
MRUE [%]	69.09	76.40	8.00	24.48	101.35	11.14	

Next, the performance of the microsolvation model used for calculation of the free energies of species **3** – **9** was tested against experimental deprotonation and reduction free energies of oxygen species in water, see Figure S10. Each oxygen species was solvated with 4 explicit water molecules and the cluster surrounded by the COSMO dielectric continuum (as described previously for **3** – **9** in section S4.2). The DFT functional is B3LYP+D3. Electronic energy and free energy corrections were calculated as explained in section S4.1. The free energy of the solvated proton, which has a transient structure (fluctuating defect), was not calculated explicitly but left as a fit parameter to align the computed deprotonation free energies to the experimental scale. For reduction reactions the reaction free energy was calculated for pH=7 vs SHE.

We found excellent agreement between computed and experimental free energies ($R^2 > 0.99$). The errors in potentials for the stepwise reduction of oxygen to water are reasonably small, in the order of 0.3 V (see table S7). Results are also given for a model where only the COSMO continuum solvation model is used, without explicit water molecules (column COSMO only). In this case errors are very large which shows that inclusion of explicit water molecules is essential. Hence, we conclude that the B3LYP+D3 functional in combination with our microsolvation model performs very well for both sets of calculations, reduction of O_2 at the di-iron active site and in aqueous solution. This approach was therefore chosen for the calculations presented in the main text.

The microsolvation model used was additionally validated by comparing the computed hydration free energies to experiment. The results are summarized in Table S6, where we also give the results for the COSMO only model, without explicit water molecules. On the basis of these data it is clear that an adequate description of solvation of charged species such as OH^- and O_2^- can only be achieved if the first hydration shell is treated explicitly as done in our microsolvation model. Similar results have been reported before in the literature by Truhlar and co-workers for redox potential calculation of aqueous ions[63] and pKa calculations.[64] The inclusion of explicit water seems to be less crucial for the solvation free energy of neutral species, which is already reasonably well described by COSMO only. Unfortunately, we could not find an experimental value for H_2O_2,

which is why this species is not included in the table.

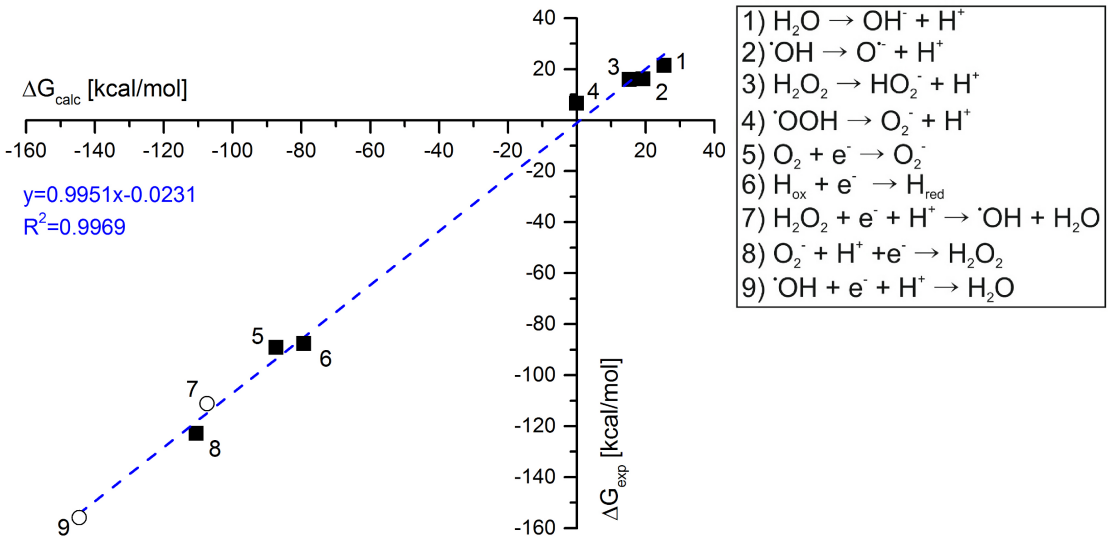

Figure S10: Correlation between experimental[65–67] and calculated reaction free energies for deprotonation and reduction reactions of oxygen species. H_{ox} and H_{red} denote oxidized (Fe(II)Fe(I)) and reduced form ((Fe(I)Fe(I)) of the active site model, respectively. Reactions denoted by a filled square are used for the fit of H^+ solvation free energy.

Table S6: Summary of experimental and computed solvation free energies, $X_{(g)} \rightarrow X_{(aq)}$ at standard conditions, X=H_2O,OH^-,O_2^-. Calculations were carried out without explicit water molecules and COSMO continuum solvation model only or with a microsolvation model where 4 water molecules are explicitly included and the remaining solvation shells modelled with a COSMO continuum solvation model. MUE denotes the mean unsigned error of the method with respect to the experimental values. All values in units of kcal/mol.

Molecule	Exp.	Only COSMO	Microsolvation
H_2O[68]	-6.3±0.4	-9.9	-5.1
OH^-[69]	-106.4±0.5	-68.9	-107.8
O_2^-[65]	-85.0	-57.3	-86.0
	MUE	22.9	1.2

Table S7: Comparison of the calculated and experimental[66,67] reduction potentials w.r.t SHE at pH=7 for set of reactions involving oxygen species (see Figure S10). The calculations employ B3LYP+D3 functional with COSMO or microsolvation models denoted as $E_{calc}^{\mathrm{COSMO}}$ or $E_{calc}^{\mathrm{microsolv.}}$, respectively. MUE denotes the mean unsigned error of the method with respect to the experimental values.

Reaction	$E_{calc}^{\mathrm{COSMO}}$ [V]	$E_{calc}^{\mathrm{microsolv.}}$ [V]	E_{exp} [V]
5	-1.53	-0.27	-0.33
6	-0.62	-0.62	-0.40
7	-0.86	0.32	0.89
8	-0.99	0.19	0.38
9	0.65	1.80	2.32
MUE [V]	1.24	0.31	–

S5 Caption of fig 2 and the site-directed mutants of Cr FeFe hydrogenase

S5.1 Caption of fig 2

A: Effect of H/D exchange on the inhibition of WT Ca FeFe hydrogenase by O_2. pH or pD = 7.1, $E = 90$ mV vs SHE, $T = 12^\circ$ C, 1 bar H_2 or D_2. (Experiment with H_2 oxidation in H_2O, $[O_2]_0 = 6.25$ μM, $\tau = 49$ s; 12.5 μM, 50 s; 25 μM, 53 s; experiment with D_2 oxidation in D_2O, $[O_2]_0 = 6.25$ μM, $\tau = 43$ s; 12.5 μM, 40 s; 25 μM, 37 s).

B: Effect of pH on the inhibition of WT Ca FeFe hydrogenase by O_2. pH = 6, 7 and 8.5, $E = 190$ mV, $T = 12^\circ$C, $[O_2]_0 = 12.5$ and 25 μM, $\tau = 38$ and 39 s at pH 6; 39 and 36 s at pH 7; 25 and 25 s at pH 8.5.

C: Effect of electrode potential on the inhibition of WT Ca FeFe hydrogenase by O_2. pH = 6, $E = 40$ and 140 mV, $T = 12^\circ$C, $[O_2]_0 = 6.25$, 12.5 and 25 μM, $\tau = 35$, 34 and 35 s at 40 mV; $\tau = 33$, 32 and 33 s at 140mV.

D: Effect of F290Y and V296F substitutions on the inhibition of Cr FeFe hydrogenase by CO. pH = 7, $E = 190$ mV, $T = 30\ ^\circ$C, $[CO]_0 = 4.8$ μM, $\tau = 19$ s (WT), 17 s (V296F) and 19 s (F234Y).

E: Effect of F290Y and V296F substitutions on the inhibition of Cr FeFe hydrogenase by O_2. pH = 7, $E = 40$ mV, $T = 12\ ^\circ$C, $[O_2]_0 = 12.5$ μM, $\tau = 38$ s (WT), 20 s (V296F) and 41 s (F234Y). The inset in panel E shows the data in a plot of $-\mathrm{d}(log(i))/\mathrm{d}t$ against the time after the injection of O_2. As explained in ref 54, this gives the instant rate constant of inactivation (provided the reaction is irreversible, which is only true just after the time of injection of O_2). The inset therefore shows that the F290Y mutant reacts with O_2 about twice as slowly as the WT enzyme.

F: Effect of C169D substitution on the inhibition of Cr FeFe hydrogenase by O_2. pH = 7, $E = 40$ mV, $T = 3^\circ$C, $[O_2]_0 = 25$ μM, $\tau = 45$ s for Cr WT and 49 s for Cr C169D. E: Cr WT and Cr V296F, pH = 7, 1 bar H_2, $\omega = 3$ krpm, $E = -158$ mV, $T = 30^\circ$C, $[CO]_0 = 2.4$ μM, $\tau = 20$ s for Cr WT and 17.5 s for Cr V296F.

S5.2 The site-directed mutants

Site-directed mutagenesis was performed on the CrhydA1 gene cloned into the pBBR-hydA1N vector[70] using Quick Change Site-Directed Mutagenesis Kit (Agilent Technologies, Santa Clara, CA, USA). The recombinant plasmids were introduced and expressed in *Shewanella oneidensis* AS52 strain as described in ref. 70.

S5.2.1 C169D

The mutagenesis primers used for creating C169D mutant were T226Kup 5'-ccatgttcaccagcg**att**-tgccccggctgga-3'.

The analysis of the C169D data recorded at pH 7, $E = 40$ mV, $T = 12°$C (ref 71 and fig S11) returns: $k_i = 2.5 \pm 0.5$ mM^{-1}s^{-1} (WT) and 3.8 ± 0.4 mM^{-1}s^{-1} (C169D); $k_a = 0.035 \pm 0.005$ s^{-1} (WT) and 0.010 ± 0.001 s^{-1} (C169D), $k_3 = 0.024 \pm 0.003$ s^{-1} (WT) and 0.0021 ± 0.0008 s^{-1} (C169D).

S5.2.2 V296F

For the V296F mutant the primers were Hyd1-830Fw 5'- TGACCGCGACTGGTTCTGTGTGGACG-3' and Hyd1V296Frev 5'- GCGCAGTGCCGCCTCCAT**GAA**ACCTCCGGTGGTGCCGAACAG -3' (with nucleotide triplets coding a mutated amino acid shown in bold, and underlined are silent base changes to lower secondary structure formation). The PCR program used was 96°C 5 min, [96°C 1 min, 65°C 3 sec, 72°C 17 min] for 25 cycles, and a final cycle at 72°C 17 min. The PCR products were digested with DpnI and directly transformed into *E. coli*, and clones were sequenced to confirm the mutation.

Figure S12 shows experiments in which films of WT Cr and V286F were exposed to series of potential steps (as shown in the upper panel), and their current response (bottom). Following each step, the equilibrium between active and anaerobically inactivated species changes, which results in a multiexponential relaxation towards a new steady-state. We analyzed the transients in detail to gain insight in the inactivation process in ref. 72. The difference between the WT and the

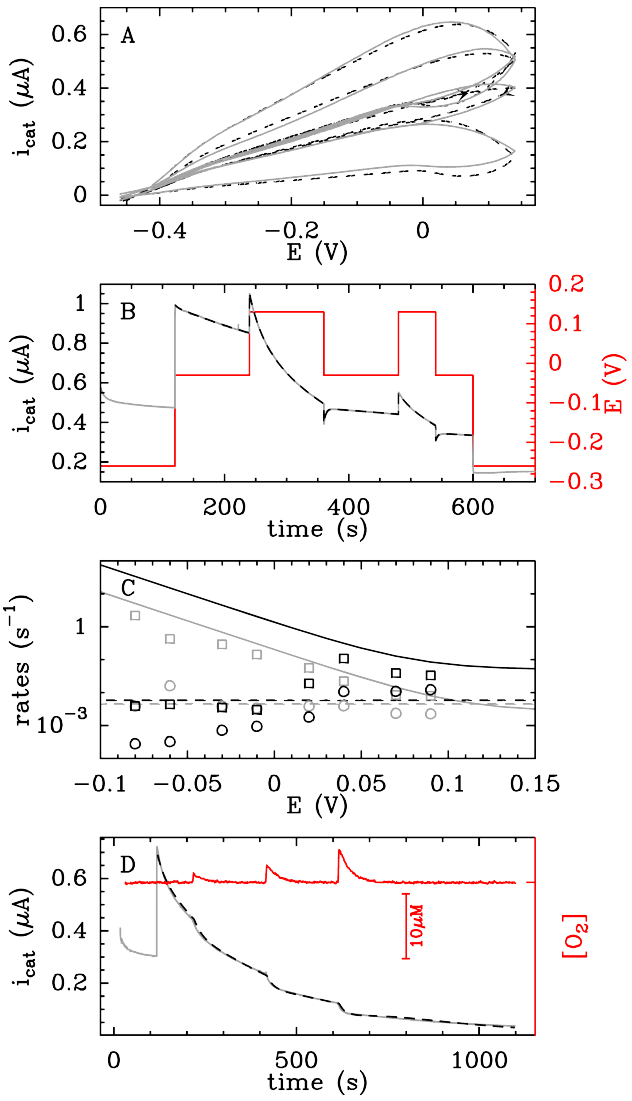

Figure S11: Characterization of the anaerobic / aerobic inactivation of C169D Cr hydrogenase grafted on rotating electrode, $T = 12°C$, pH = 7, $\omega = 3000$ rpm, 1 bar H_2. A: Cyclic voltammograms at different scan rates (5, 10, 20 and 2 mV/s; gray lines) and fits (dashed black lines). B: Current response of H_2-oxidation (gray line) and fit (black dashed line) for a sequence of potential steps applied to the electrode (red line). C: Potential dependence of the rate constants for the anaerobic inactivation, extracted from fits shown on panels A (k_a: plain lines and k_i: dashed lines) and B (k_a: square dots and k_i: circle dots). The rate constants for two species involved in the kinetic model are distinguished using black and gray plots. D: Catalytic current of H_2-oxidation changes with enzyme exposure to O_2 (gray line) , $E = 40$ mV; $[O_2]_0 = 1.25$ μM, $\tau = 31$ s; 2.5 μM, 30 s; 5 μM, 30 s. The oxygen reduction current is plot against time as a red line, $E = -560$ mV; $\omega = 6000$ rpm.

V296F is most visible in the steps at ≈ 0.05 V at $t = 150$ s and 350 s: whereas the WT enzyme quickly inactivates or activates (and then irreversibly inactivates), the inactivation/activation of the V296F mutant is very slow (neither are complete in these steps). Surprisingly, the rate of inactivation/reactivation is slower at 0.05 V than at 0.15 V. This is not compatible with the model that explains the data in the WT enzyme, for which the relaxation rate increases when the potential is decreased. This shows that the chemistry of the anaerobic inactivation in the V296F mutant is not the same as that in the WT enzyme, which suggests that the aerobic inactivation may be different too. Hence, the difference in O_2 reaction rate between the WT and the V296F (main text fig 2E) cannot be interpreted only in terms of kinetics of diffusion along the gas channel.

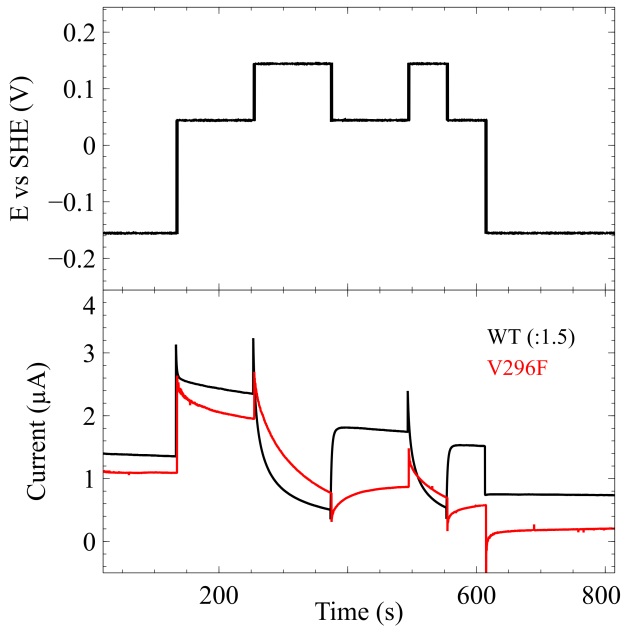

Figure S12: Anaerobic (in)activation of WT and V296F Cr FeFe hydrogenase.

S5.2.3 F290Y

The construction and partial characterization of the F290Y mutant are described in ref 72, although this mutant was mistakenly called F234Y therein.

S5.2.4 F290W

The mutagenesis primers used for creating the F290W mutant were Hyd1-830Fw 5'- TGACCGCGA-CTGGTTCTGTGTGGACG-3' and Hyd1F290Wrev 5'- CTCCATGACACCGCCAGTGGTGCC-**CCA**CAGCACGCCTGCGCCCGAG -3', (with nucleotide triplets coding a mutated amino acid shown in bold, and underlined are silent base changes to lower secondary structure formation).

S6 XYZ coordinates of computed structures, Fig. 5 main text

State 1
80

C	2.8858334	33.3821088	28.4303703
S	1.6505058	32.1597973	29.0114418
Fe	0.1734620	31.5501570	27.3448925
Fe	-2.2501140	30.8211592	27.1631377
C	-2.6696533	29.0472011	26.6944106
N	-2.7762916	27.8864933	26.4937650
C	0.6660615	33.0439297	26.2920597
N	1.0099502	33.9762706	25.6679402
C	-1.6726493	32.7772929	29.9511966
S	-1.6508144	32.8321548	28.0783278
C	-0.9782849	30.5044836	30.4237514
S	-0.7650168	29.8991147	28.6498285
C	1.4086597	30.6026160	26.5732433
O	2.2310410	30.0187186	25.9916107
C	-3.4748560	31.5965561	26.1689105
O	-4.2909424	32.1125816	25.5220737
C	-0.9485221	30.9446056	25.7942629
O	-0.8097855	30.7267767	24.6443231
N	-1.9405438	31.5319373	30.6115553
H	-2.8838290	31.1760963	30.4267139
H	2.3374527	34.2351996	28.0176129
H	3.5131265	32.9425967	27.6481550
H	-0.6816747	33.1445902	30.2567916
H	-2.4353111	33.5126656	30.2342250
H	0.0162866	30.8374414	30.7504531
H	-1.2686988	29.6073861	30.9830858
C	-9.4623550	19.8487551	23.3205802
N	-9.0294116	19.7113824	21.8767463
H	-8.8712985	19.1490683	23.9192259
H	-10.5278967	19.6064351	23.3787934
H	-8.0061822	19.9347739	21.7645665
H	-9.1857756	18.7281284	21.5256844
H	-9.5721755	20.3659848	21.2545947
C	-4.7072237	27.7904542	30.1710166
S	-4.7447636	29.4185366	30.9981489
C	0.2291980	27.1926574	32.5064788
S	1.9984643	26.7232696	32.4154416
C	6.9139297	31.4752476	32.9484591
S	6.7267475	29.7104495	32.4930716
H	-5.5334749	30.0405294	30.0923016
H	-4.3068889	27.8779338	29.1537514
H	-5.7021209	27.3304321	30.1610429
H	0.1172186	28.1568155	33.0181576
H	-0.2994722	26.4176022	33.0779012
H	6.5566324	32.1368047	32.1498033
H	7.9804345	31.6734269	33.1232625
Fe	2.9225888	28.1984342	31.0915289
Fe	5.0331887	29.6205928	31.1144447
S	4.9576976	27.4186232	30.7272787
S	3.0841105	30.2084471	32.0373961
C	5.2682754	28.8894859	25.8077522
S	5.0938211	27.5352706	27.0376919
C	0.7216845	27.0683127	26.3273091
N	-0.3211679	27.0832559	27.3886311
H	4.4141355	29.5698979	25.8466137
H	5.3231497	28.4372666	24.8081890
H	1.7144455	27.1570108	26.7814153
H	0.5425499	27.9231298	25.6683818
H	-0.2366122	27.9526351	27.9929626
H	-1.3184127	27.1774516	26.9868091
C	9.0870818	25.2234985	20.2240736
N	10.5874728	25.3921132	20.1158233
H	-0.2484676	26.2728850	28.0107618
H	8.7082331	25.9803648	20.9173042
H	8.6576866	25.3608151	19.2270023
H	11.0023684	24.6821872	19.4567481
H	10.8383811	26.3473324	19.7565491
H	11.0507230	25.2709860	21.0504976
Fe	2.9302030	30.4685704	29.8416921
Fe	4.3415271	28.4395799	28.8851936
S	5.0620559	30.5567069	29.1540051
S	2.1005312	28.5064738	29.1397422
H	-0.2097949	27.2673035	31.5027349
H	-4.0316849	27.1637136	30.7663397
H	-9.2780152	20.8808871	23.6327980
H	8.8849174	24.2167167	20.6007240
H	6.1925987	29.4449165	26.0124723
H	6.3500249	31.6819857	33.8671499
H	0.6392148	26.1376942	25.7557892
H	3.4992289	33.6735061	29.2907136

State 2
82

C	2.8858334	33.3821088	28.4303703
S	1.6864124	32.2088114	29.1592025
Fe	0.1063307	31.5905805	27.5659632
Fe	-2.3641944	30.9368312	27.6039728
C	-2.6273356	29.2150732	26.8646608
N	-2.6392689	28.0964517	26.4910395
C	0.5476593	33.1182181	26.5261582
N	0.8434054	34.0552383	25.8866336
C	-1.5332732	32.7458178	30.3588026
S	-1.5915494	32.9033159	28.4880106
C	-0.8733889	30.4401707	30.6879937
S	-0.7391939	29.9098904	28.8796569
C	1.3399349	30.6708016	26.7393393
O	2.1543807	30.1262692	26.1138714
C	-3.4432708	31.7957293	26.4898778
O	-4.1386590	32.3442834	25.7495049
C	-0.9940885	31.1226829	26.0890838
O	-1.0190737	30.9469278	24.9298886
N	-1.8065579	31.4746211	30.9555110
H	-2.7630211	31.1537136	30.7852050
H	2.3265593	34.2522417	28.0732042
H	3.4131994	32.9194177	27.5900988
H	-0.5242460	33.0791724	30.6414001
H	-2.2712146	33.4800838	30.7037496
H	0.1422184	30.7289758	30.9942252
H	-1.1735557	29.5242747	31.2087096
C	-9.4623550	19.8487551	23.3205802
N	-8.9887849	19.8461818	21.8832419
H	-8.8684179	19.1152766	23.8742576
H	-10.5225148	19.5779668	23.3284788
H	-7.9698163	20.1030960	21.8190919
H	-9.1092494	18.8937654	21.4452606
H	-9.5315965	20.5377961	21.3037689
C	-4.7072237	27.7904542	30.1710166
S	-4.7860706	29.0652508	31.4781495
C	0.2291980	27.1926574	32.5064788
S	1.9725905	26.6543176	32.3374464
C	6.9139297	31.4752476	32.9484591
S	6.6681934	29.6911397	32.6235581
H	-5.2474443	30.0454750	30.6538360
H	-4.0738865	28.1293441	29.3436279
H	-5.7096732	27.5483597	29.7997988
H	0.1751970	28.1253366	33.0809649
H	-0.3165881	26.4062887	33.0441802
H	7.0330272	32.0344047	32.0124893
H	7.8244250	31.5816373	33.5527366
Fe	2.9235204	28.1525108	31.0675270
Fe	5.0256234	29.5818382	31.1924510
S	4.9739647	27.3959906	30.7471605
S	3.0490016	30.1247760	32.0765474
C	5.2682754	28.8894859	25.8077522
S	5.2206149	27.5717381	27.0866471
C	0.7216845	27.0683127	26.3273091
N	-0.3142711	27.1233552	27.3922337
H	4.2884236	29.3617300	25.6932792
H	5.5664279	28.4251741	24.8582105
H	1.7209380	27.0278518	26.7753826
H	0.6328112	27.9761561	25.7240342
H	-0.1508833	27.9317303	28.0478325
H	-1.3073647	27.3375468	26.9810736
C	9.0870818	25.2234985	20.2240736
N	10.5757820	25.4940351	20.2553162
H	-0.3275415	26.2718357	27.9609292
H	8.5980936	25.9341428	20.8971169
H	8.7395205	25.3588854	19.1954643
H	11.0952423	24.8315329	19.6212216
H	10.7903393	26.4737845	19.9402297
H	10.9620786	25.3787585	21.2253317
Fe	2.9581659	30.4557156	29.8940592
Fe	4.4084970	28.4595366	28.9151718
S	5.1028560	30.5751185	29.2642728
S	2.1651652	28.5180784	29.0978349
H	-0.2341871	27.3470849	31.5235667
H	-4.2682378	26.8952829	30.6284862
H	-9.3140251	20.8546642	23.7249822

H	8.9223950	24.1950401	20.5592211
H	6.0063900	29.6492368	26.0917168
H	6.0607513	31.8794700	33.5071886
H	0.5408241	26.1907915	25.6974296
H	3.5967088	33.6559308	29.2187837
O	-3.7426530	30.6094896	28.8615781
O	-4.9959897	30.9240888	28.6921183

State 3

83

C	2.8858334	33.3821088	28.4303703
S	1.6839330	32.1915613	29.1204974
Fe	0.1615418	31.5841835	27.5098154
Fe	-2.2841594	30.9991639	27.4227415
C	-2.6208814	29.2585965	26.7671394
N	-2.7071014	28.1206431	26.4633249
C	0.6541428	33.0641984	26.4225397
N	0.9840503	33.9765998	25.7642700
C	-1.5838998	32.8257646	30.1893120
S	-1.5182590	32.9584601	28.3231907
C	-1.0143322	30.5071301	30.5948444
S	-0.7582846	29.9505841	28.8103129
C	1.3784917	30.6210998	26.7078686
O	2.1907606	30.0590591	26.0943140
C	-3.3193859	31.9042045	26.3068311
O	-3.9958076	32.4894802	25.5776475
C	-0.9616538	31.0687194	25.9825344
O	-0.8784853	30.8703359	24.8275945
N	-1.9441197	31.5659933	30.7663889
H	-2.8769073	31.2707253	30.4623579
H	2.3272503	34.2563101	28.0819327
H	3.4236730	32.9383001	27.5866310
H	-0.5852337	33.1271629	30.5381526
H	-2.3174887	33.5866313	30.4817158
H	-0.0186174	30.7810759	30.9725611
H	-1.3780144	29.6073819	31.1039612
C	-9.4623550	19.8487551	23.3205802
N	-9.1766769	19.7021988	21.8413092
H	-8.8221850	19.1450536	23.8611498
H	-10.5196992	19.6201499	23.4855636
H	-8.1660428	19.9081405	21.6278903
H	-9.3840448	18.7220623	21.5109712
H	-9.7664047	20.3646425	21.2735781
C	-4.7072237	27.7904542	30.1710166
S	-4.6512128	29.1486706	31.3863065
C	0.2291980	27.1926574	32.5064788
S	1.9895019	26.6945989	32.3948686
C	6.9139297	31.4752476	32.9484591
S	6.7363803	29.7034534	32.5147947
H	-4.7725094	30.1297492	30.4570737
H	-3.9537557	27.9490384	29.3894817
H	-5.7029633	27.6983788	29.7219508
H	0.1391998	28.1549222	33.0251065
H	-0.3039543	26.4242297	33.0814228
H	6.4737382	32.1211707	32.1802313
H	7.9842937	31.7038875	33.0368203
Fe	2.9359102	28.1717258	31.0962103
Fe	5.0538047	29.5918219	31.1345746
S	4.9711312	27.3960492	30.7320106
S	3.1104278	30.1676688	32.0602350
C	5.2682754	28.8894859	25.8077522
S	5.1099119	27.5367744	27.0415858
C	0.7216845	27.0683127	26.3273091
N	-0.3373872	27.1585314	27.3690725
H	4.4151922	29.5710709	25.8597741
H	5.3107842	28.4368684	24.8080605
H	1.7099981	27.0429979	26.8006316
H	0.6486380	27.9564427	25.6936637
H	-0.1899686	27.9888992	28.0060367
H	-1.3188740	27.3500840	26.9478069
C	9.0870818	25.2234985	20.2240736
N	10.5828438	25.4270536	20.1190367
H	-0.3571533	26.3270432	27.9666882
H	8.6905332	25.9693956	20.9195466
H	8.6556449	25.3528350	19.2268883
H	11.0144509	24.7296509	19.4576721
H	10.8109356	26.3898736	19.7634659
H	11.0482104	25.3129788	21.0538123
Fe	2.9577659	30.4503296	29.8745996
Fe	4.3662765	28.4337036	28.8968547
S	5.0797471	30.5469386	29.1850662
S	2.1223481	28.5029700	29.1405143
H	-0.2208715	27.2794292	31.5094020
H	-4.4710503	26.8662747	30.7136969
H	-9.2378542	20.8800411	23.6089254
H	8.9077003	24.2111513	20.5984138
H	6.1952441	29.4438220	25.9999527
H	6.4189028	31.6658729	33.9091821
H	0.5557753	26.1693978	25.7241512
H	3.5877363	33.6473262	29.2299820
O	-3.7778724	30.7996047	28.6512181
O	-5.0288505	30.3460433	28.0480420
H	-4.7671555	29.4572742	27.7218123

State 4

84

C	2.8858326	33.3820994	28.4303623
S	1.6219511	32.2635335	29.0964154
Fe	0.0399553	31.9061225	27.4293173
Fe	-2.3871297	31.1898245	27.4843194
C	-2.4469966	29.6476301	26.3909834
N	-2.3603012	28.6400186	25.7910581
C	0.5745360	33.5437028	26.6157101
N	0.9129015	34.5464889	26.1128649
C	-1.5557582	32.7992925	30.3466329
S	-1.6497037	33.1149377	28.4995451
C	-0.8661414	30.4913960	30.4558991
S	-0.7267084	30.1129927	28.6091636
C	1.2264459	30.9652401	26.5479734
O	2.0085224	30.3572909	25.9436131
C	-3.6251000	32.0828099	26.5766297
O	-4.4467131	32.6556092	26.0034744
C	-1.0535589	31.8248941	25.9243153
O	-1.1917141	31.9310073	24.7699361
N	-1.8288036	31.4734871	30.8058570
H	-2.7658168	31.1724110	30.5113185
H	2.4067028	34.3282768	28.1632084
H	3.3555827	32.9500495	27.5408910
H	-0.5436374	33.1044582	30.6477187
H	-2.2929217	33.4983451	30.7602788
H	0.1397369	30.7786896	30.7909884
H	-1.1546895	29.5145083	30.8615124
C	-9.4623523	19.8487495	23.3205737
N	-9.3655791	20.2047477	21.8525711
H	-8.7293859	19.0630602	23.5272904
H	-10.4791885	19.4950998	23.5166741
H	-8.4028951	20.5534825	21.6091631
H	-9.5676387	19.3658131	21.2444598
H	-10.0539353	20.9593803	21.5984747
C	-4.7072224	27.7904464	30.1710081
S	-2.9449890	27.8252796	29.6701643
C	0.2291979	27.1926498	32.5064697
S	1.9646171	26.6710948	32.2588397
C	6.9139278	31.4752388	32.9484498
S	6.5370724	29.7086103	32.6529129
H	-3.3128400	29.6542492	29.0143586
H	-5.3441011	28.0526396	29.3161371
H	-4.8931675	28.5082449	30.9794964
H	0.1960905	28.1655168	33.0122005
H	-0.2545133	26.4410228	33.1441333
H	7.1365504	31.9938462	32.0079470
H	7.7930370	31.5196479	33.6044448
Fe	2.8394027	28.1911958	30.9796029
Fe	4.9346108	29.6352780	31.1690892
S	4.8992206	27.4490933	30.7131507
S	2.9262048	30.1552788	31.9983288
C	5.2682739	28.8894778	25.8077450
S	5.2635143	27.5890457	27.1028428
C	0.7216843	27.0683051	26.3273017
N	-0.4804847	27.2831991	27.1776726
H	4.2710725	29.3241865	25.6800461
H	5.5878704	28.4282264	24.8635332
H	1.5659166	26.7374342	26.9402528
H	0.9760503	28.0217555	25.8549584
H	-0.3172909	28.0419734	27.8834361
H	-1.3071307	27.6649471	26.5913160
C	9.0870792	25.2234914	20.2240679
N	10.3308071	25.8701479	20.7962914
H	-0.7912272	26.4532105	27.6944499
H	8.2155426	25.7241035	20.6564233
H	9.1101937	25.3489074	19.1372048
H	11.2036957	25.4205610	20.4108944
H	10.3674435	26.8948811	20.5624384
H	10.3585810	25.7800942	21.8422056
Fe	2.8888736	30.4893041	29.8150980
Fe	4.3639078	28.4996087	28.8754200

S	5.0541089	30.6187969	29.2370252
S	2.1098870	28.5620251	28.9941750
H	-0.3189881	27.2555086	31.5572044
H	-4.9734511	26.7813271	30.5143567
H	-9.2436935	20.7486506	23.9032934
H	9.1017052	24.1635818	20.4953371
H	5.9728853	29.6832359	26.0841628
H	6.0685110	31.9676445	33.4445905
H	0.4843101	26.3273768	25.5564817
H	3.6414094	33.5288639	29.2120256
O	-3.6848123	30.5310406	28.6462440
O	-6.2367632	30.0317044	27.7770457
H	-5.3036517	30.2013760	28.0837700
H	-6.5764785	30.9200933	27.5857555

State 5

84

C	2.8858326	33.3820994	28.4303623
S	1.7794841	32.1588731	29.1906379
Fe	0.1562191	31.5219553	27.6524776
Fe	-2.3458002	31.0144212	27.7828490
C	-2.7721378	29.2281453	27.3426400
N	-2.8484594	28.0677533	27.1275861
C	0.6355594	32.9001080	26.4411905
N	0.9598828	33.7441219	25.6941081
C	-1.2979797	33.1291842	30.2803251
S	-1.4523269	33.0305021	28.4197837
C	-0.7336218	30.8381639	30.8829051
S	-0.7622100	30.0369823	29.1771531
C	1.3483578	30.5341600	26.8463630
O	2.1318650	29.9834684	26.1860765
C	-3.3611151	31.8361186	26.5936348
O	-3.9888578	32.3795402	25.7848492
C	-1.0273610	30.8680720	26.3117931
O	-1.0548186	30.4815875	25.1962405
N	-1.5843336	31.9674427	31.0752818
H	-2.5735566	31.7229709	31.0198823
H	2.2739622	34.2234312	28.0891736
H	3.4042179	32.9486065	27.5689674
H	-0.2570743	33.4361825	30.4579612
H	-1.9746634	33.9414969	30.5709221
H	0.3118307	31.1157016	31.0706866
H	-1.0165124	30.0296406	31.5668961
C	-9.4623523	19.8487495	23.3205737
N	-9.3096494	19.7593679	21.8173713
H	-8.7705404	19.1319382	23.7736963
H	-10.4989747	19.6019171	23.5699956
H	-8.3216014	19.9896326	21.5228061
H	-9.5340410	18.7848932	21.4712694
H	-9.9598169	20.4352155	21.3300240
C	-4.7072224	27.7904464	30.1710081
S	-3.3954085	28.6017197	31.1466017
C	0.2291979	27.1926498	32.5064697
S	1.9481135	26.5891923	32.3006518
C	6.9139278	31.4752388	32.9484498
S	6.7118155	29.6777970	32.6648360
H	-4.1679407	28.9799617	32.1935640
H	-4.2482442	27.5732038	29.1973438
H	-5.5495900	28.4713516	30.0214933
H	0.2108162	28.0514400	33.1895779
H	-0.3690575	26.3783282	32.9362121
H	7.0738829	32.0072905	32.0026928
H	7.7890824	31.6153229	33.5968129
Fe	2.9544234	28.1289168	31.1068349
Fe	5.0837624	29.5292039	31.2251670
S	5.0057380	27.3452964	30.7651602
S	3.1304320	30.0987994	32.1383434
C	5.2682739	28.8894778	25.8077450
S	5.2216207	27.5652826	27.0811207
C	0.7216843	27.0683051	26.3273017
N	-0.2034170	27.2864536	27.4798488
H	4.2944023	29.3782436	25.7134739
H	5.5412462	28.4246114	24.8509413
H	1.7532011	27.0453025	26.6975027
H	0.6003321	27.9041787	25.6332294
H	0.0909265	28.1154412	28.0496687
H	-1.2283109	27.4696672	27.2125411
C	9.0870792	25.2234914	20.2240679
N	10.5272526	25.6540524	20.4001301
H	-0.1732740	26.4977147	28.1348840
H	8.4606738	25.8715468	20.8444474
H	8.8297993	25.3291666	19.1657869
H	11.1759536	25.0547783	19.8200523
H	10.6628956	26.6560603	20.1039364
H	10.8264798	25.5728743	21.4054434
Fe	3.0404169	30.4500240	29.9574674
Fe	4.4511836	28.4395653	28.9406620
S	5.1656478	30.5455012	29.3079590
S	2.1965470	28.5291910	29.1315571
H	-0.2074635	27.4924060	31.5449583
H	-5.0219989	26.8589686	30.6543162
H	-9.2196092	20.8713270	23.6254290
H	9.0044691	24.1802230	20.5438245
H	6.0245565	29.6351953	26.0811830
H	6.0261643	31.8819652	33.4482732
H	0.4589712	26.1268000	25.8339038
H	3.6129413	33.6996454	29.1873108
O	-3.8467708	31.0597616	29.2964294
O	-5.1852524	30.6440525	28.7892889
H	-4.8940632	30.2156334	27.9505211
H	-3.6329699	30.2780436	29.9027788

State 6

85

C	2.8858318	33.3820900	28.4303543
S	1.7738452	32.1353825	29.1338205
Fe	0.1707662	31.6333738	27.5812979
Fe	-2.2358038	30.9854733	27.6596714
C	-2.5642266	29.2875397	26.9143135
N	-2.6437759	28.1776213	26.5216458
C	0.5873917	33.1553279	26.5192835
N	0.8585819	34.0935403	25.8700039
C	-1.3812071	32.7927372	30.4054023
S	-1.4523766	32.9694183	28.5473554
C	-0.7933339	30.4745703	30.6985396
S	-0.5903351	29.9493086	28.8896978
C	1.3163885	30.7107535	26.6362220
O	2.0746683	30.1730139	25.9363072
C	-3.4264520	31.9105460	26.7249987
O	-4.2004906	32.5185745	26.1233737
C	-1.0883681	31.1855038	26.1131250
O	-1.0807033	31.0678565	24.9453194
N	-1.7346694	31.5097647	30.9422520
H	-2.6553816	31.2363299	30.5574954
H	2.2855804	34.2575980	28.1624985
H	3.3745669	33.0037485	27.5262092
H	-0.3572265	33.0638073	30.7011849
H	-2.0817623	33.5531562	30.7722853
H	0.2127512	30.7514797	31.0426791
H	-1.1132036	29.5459711	31.1852248
C	-9.4623496	19.8487439	23.3205672
N	-9.3450724	20.4591537	21.9399330
H	-8.7284806	19.0406073	23.3972997
H	-10.4802354	19.4633836	23.4347583
H	-8.3802668	20.8479686	21.7777981
H	-9.5351204	19.7395824	21.1901408
H	-10.0336855	21.2457399	21.8136440
C	-4.7072211	27.7904386	30.1709996
S	-2.9273384	27.4012478	30.0204673
C	0.2291978	27.1926422	32.5064606
S	1.8487687	26.5176082	31.9681317
C	6.9139259	31.4752300	32.9484405
S	6.6802447	29.7047423	32.5350914
H	-3.3619330	29.6996803	29.2857362
H	-5.0658370	28.0586242	29.1664459
H	-4.8511046	28.6518939	30.8319339
H	0.3715886	28.0453158	33.1815870
H	-0.3155251	26.3971035	33.0323876
H	7.0922676	32.0573005	32.0350586
H	7.7867542	31.5574647	33.6095285
Fe	2.9027920	28.0943769	30.9277798
Fe	4.9905598	29.5613809	31.2171854
S	4.9478728	27.4601267	30.6852337
S	2.9923255	30.0113067	31.9378647
C	5.2682724	28.8894697	25.8077378
S	5.3420671	27.6247120	27.1353372
C	0.7216841	27.0682975	26.3272943
N	-0.3082893	27.1357513	27.4003263
H	4.2513609	29.2786061	25.6945949
H	5.5830341	28.4152459	24.8678195
H	1.7137258	26.9168473	26.7654089
H	0.7088446	28.0182038	25.7865269
H	-0.1173710	27.9272155	28.0685477
H	-1.2913217	27.3788840	27.0027818
C	9.0870766	25.2234843	20.2240622
N	9.9740274	26.0338815	21.1465328

H	-0.3560948	26.2760412	27.9552235
H	8.0544571	25.5515681	20.3759436
H	9.4092200	25.4102420	19.1949707
H	10.9852958	25.7550656	21.0400758
H	9.9014965	27.0614148	20.9380516
H	9.7071994	25.8932708	22.1520872
Fe	3.0129913	30.4017543	29.8035572
Fe	4.4771890	28.5558118	28.8965823
S	5.1203321	30.6130254	29.3345157
S	2.2821747	28.5568101	28.9109894
H	-0.3557053	27.5199869	31.6372921
H	-5.2601729	26.9215287	30.5472878
H	-9.2571079	20.6322842	24.0561640
H	9.2031122	24.1670495	20.4846199
H	5.9471990	29.7188126	26.0416790
H	6.0306358	31.8740104	33.4627428
H	0.4658635	26.2511576	25.6438927
H	3.6368165	33.6313077	29.1901258
O	-3.6297895	30.5979977	29.0065439
O	-5.7440884	29.5397396	27.6375722
H	-5.0404467	30.0450816	28.1445133
H	-5.2540875	29.2034938	26.8672373
H	-2.6798159	27.2408129	31.3414962

State 7

86

C	2.8858318	33.3820900	28.4303543
S	1.7054700	32.2355971	29.1818814
Fe	0.1636994	31.5285130	27.6360562
Fe	-2.2042823	30.6666140	27.7319477
C	-2.5961016	28.8617961	27.3861447
N	-2.6845507	27.6968111	27.2108630
C	0.4605769	33.0222861	26.5118668
N	0.6919364	33.9551614	25.8389050
C	-1.4997812	32.8478056	30.3300142
S	-1.6602241	32.7682354	28.4641756
C	-0.6859070	30.6324436	30.8734200
S	-0.5585062	29.8937486	29.1309931
C	1.4112957	30.7430102	26.7009981
O	2.2096072	30.3425038	25.9549947
C	-3.4516247	31.3078768	26.6724149
O	-4.2476763	31.7230783	25.9357556
C	-0.9936097	30.7179966	26.2591295
O	-0.9482222	30.3675452	25.1324527
N	-1.6647273	31.6380343	31.0771164
H	-2.6131359	31.2669633	30.9969012
H	2.3242485	34.2258747	28.0133506
H	3.4381914	32.8929655	27.6208701
H	-0.4963892	33.2589233	30.5137412
H	-2.2595850	33.5759033	30.6373272
H	0.3129458	31.0209079	31.1017452
H	-0.8932721	29.7614623	31.5027003
C	-9.4623496	19.8487439	23.3205672
N	-9.1393229	21.0656407	22.4804448
H	-8.7159794	19.0791125	23.1008892
H	-10.4662368	19.5079911	23.0490743
H	-8.1791294	21.4361306	22.7031579
H	-9.1653242	20.8322039	21.4502148
H	-9.8315191	21.8405423	22.6534570
C	-4.7072211	27.7904386	30.1709996
S	-3.7170101	28.8948080	31.2319521
C	0.2291978	27.1926422	32.5064606
S	1.1657614	26.7108575	30.9970172
C	6.9139259	31.4752300	32.9484405
S	5.8659303	30.0074583	33.2775850
H	-4.4271338	30.7812547	30.0738891
H	-4.0349033	27.4985273	29.3543089
H	-5.5631111	28.3201791	29.7353150
H	0.7453487	28.0044019	33.0278342
H	0.1483651	26.3217593	33.1687704
H	7.5173681	31.3165212	32.0472709
H	7.5727101	31.6115660	33.8158550
Fe	2.8779580	28.0154467	30.5962602
Fe	4.7014461	29.5762377	31.4908893
S	5.0227496	27.4722948	30.8913811
S	2.5292338	29.7877548	31.8331688
C	5.2682724	28.8894697	25.8077378
S	6.0266033	28.0985883	27.2848474
C	0.7216841	27.0682975	26.3272943
N	0.0129251	27.1627251	27.6363019
H	4.2210509	28.5847627	25.7035378
H	5.8381413	28.5738251	24.9230956
H	1.7990567	27.1528761	26.4961304
H	0.3765844	27.8947930	25.6974321
H	0.1999111	28.0708902	28.1327880
H	-1.0479208	27.1629402	27.5016951
C	9.0870766	25.2234843	20.2240622
N	8.4376014	25.9134569	21.4066809
H	0.2944238	26.4443005	28.3190709
H	8.3349337	25.1253714	19.4353083
H	9.9246571	25.8435652	19.8899895
H	9.1179864	26.0337808	22.1978085
H	8.0834826	26.8673800	21.1424921
H	7.6209478	25.3593481	21.7699914
Fe	2.9342325	30.4517483	29.7824758
Fe	4.8895694	28.7043231	29.0530471
S	5.1381406	30.8132146	29.7826602
S	2.7577682	28.6161618	28.5360375
H	-0.7766224	27.5172667	32.2097335
H	-5.0126215	26.9021460	30.7351929
H	-9.4212890	20.1435677	24.3735590
H	9.4359242	24.2409613	20.5560942
H	5.3030634	29.9815818	25.8923386
H	6.2921874	32.3683869	32.8155610
H	0.4722386	26.1112458	25.8566299
H	3.5815981	33.7122296	29.2105892
O	-4.7935258	31.5907291	29.6420846
O	-6.3256545	29.7541639	28.0671125
H	-5.9104825	30.5274271	28.5184578
H	-5.6682123	29.5065823	27.3949718
H	-4.6689719	29.1635090	32.1567372
H	-4.0612968	31.8930368	29.0582969

State 9

84

C	2.8858318	33.3820900	28.4303543
S	1.6558741	32.2270217	29.1067438
Fe	0.0322353	31.7792566	27.5344283
Fe	-2.4348823	31.1613772	27.5837021
C	-2.9379816	29.4950115	26.9249864
N	-3.1184768	28.3897572	26.5337104
C	0.4789923	33.3342805	26.5416316
N	0.7867508	34.2973716	25.9470019
C	-1.4335317	32.8589888	30.4296317
S	-1.6444720	33.0698322	28.5734339
C	-0.8355990	30.5253404	30.6288556
S	-0.8188375	30.0753665	28.7912774
C	1.1756704	30.8306754	26.6290723
O	1.9403163	30.2307342	25.9849005
C	-3.6811014	32.0582664	26.7265298
O	-4.5026129	32.6416385	26.1475903
C	-1.2231436	31.3688581	26.0842424
O	-1.2495393	31.2371249	24.9148735
N	-1.7083606	31.5773127	31.0073006
H	-2.6923041	31.3172815	30.8671614
H	2.3509370	34.2670175	28.0699208
H	3.4224084	32.9225981	27.5934476
H	-0.3899281	33.1426755	30.6290688
H	-2.1073413	33.6087706	30.8614324
H	0.2068555	30.7636394	30.8817263
H	-1.1265616	29.5886713	31.1179914
C	-9.4623496	19.8487439	23.3205672
N	-8.9487222	21.2458996	23.0452917
H	-8.7407946	19.1365986	22.9083259
H	-10.4362753	19.7449172	22.8321199
H	-8.0091051	21.4000886	23.4966005
H	-8.8411122	21.4128804	22.0081171
H	-9.6113324	21.9735027	23.4227445
C	-4.7072211	27.7904386	30.1709996
S	-2.9352555	27.6686386	29.8978331
C	0.2291978	27.1926422	32.5064606
S	1.9555572	26.6351601	32.2681231
C	6.9139259	31.4752300	32.9484405
S	6.5386385	29.7030815	32.6840952
H	-3.0947020	27.2677648	27.7506481
H	-5.1403252	26.8106486	30.4138212
H	-5.2122341	28.2295712	29.3019116
H	0.2126615	28.1569025	33.0296328
H	-0.2857210	26.4414367	33.1197590
H	7.1732163	31.9676060	32.0031693
H	7.7688074	31.5333929	33.6347688
Fe	2.8509669	28.1561428	30.9920373
Fe	4.9367102	29.6044331	31.2001143
S	4.9152858	27.4228002	30.7227649
S	2.9210370	30.1122122	32.0316131
C	5.2682724	28.8894697	25.8077378

S	5.2773520	27.5885915	27.1028515
C	0.7216841	27.0682975	26.3272943
N	-0.4516240	27.4674427	27.1455544
H	4.2675255	29.3188855	25.6859216
H	5.5861625	28.4326343	24.8600719
H	1.5164417	26.7073791	26.9873006
H	1.0851123	27.9486801	25.7893855
H	-0.2400401	28.2525247	27.8277910
H	-1.2690282	27.8251193	26.5912211
C	9.0870766	25.2234843	20.2240622
N	8.4760291	25.8481698	21.4624329
H	-0.8496183	26.7090841	27.7226548
H	8.3063034	25.1540357	19.4602640
H	9.9044270	25.8694613	19.8890315
H	9.1861432	25.9415709	22.2310166
H	8.0993250	26.8078261	21.2571240
H	7.6820765	25.2659886	21.8310604
Fe	2.8923484	30.4680427	29.8487816
Fe	4.3745457	28.4858751	28.8883443
S	5.0579825	30.6044472	29.2793436
S	2.1211754	28.5443508	29.0080871
H	-0.2968766	27.2864930	31.5479945
H	-4.8355149	28.4696806	31.0261759
H	-9.5538686	19.7295656	24.4045550
H	9.4586185	24.2306678	20.4951941
H	5.9694079	29.6879297	26.0797068
H	6.0540226	31.9850100	33.4001286
H	0.4186947	26.2878761	25.6206655
H	3.5895868	33.6357859	29.2316931
O	-2.8707289	26.6734728	28.5541247
O	-4.3792385	30.8093752	29.8446827
H	-4.3195533	31.5216076	29.1726484
H	-3.8757515	30.0724715	29.4285904

H2O2(H2O)4

16

O	-2.1916665	0.9923113	-0.7054710
H	-2.3394370	1.8819446	-0.2400365
O	-0.7427122	1.0093232	-0.9387358
H	-0.3965537	0.5356233	-0.1104799
O	-0.0317692	-0.4164070	1.2010720
H	-0.8997652	-0.9183402	1.1883223
H	-0.0034537	0.0286537	2.0637816
O	-2.5309035	-1.2796699	0.7705986
H	-2.6716590	-2.0422528	0.1858765
H	-2.5815154	-0.4767920	0.1811979
O	-0.1602771	3.6861013	-1.0648525
H	0.7090470	3.8778319	-0.6780984
H	-0.2148952	2.6930040	-1.1359305
O	-2.3763945	3.4187112	0.4019359
H	-1.5519979	3.7456582	-0.0653258
H	-3.1080138	3.9471138	0.0427281

O2(H2O)4

14

O	-2.4874333	2.1197185	2.2214244
O	-1.3411987	2.1800270	2.6347344
O	0.1873231	0.1505444	0.3103856
H	0.2591486	0.0097956	1.2681598
H	-0.7415402	-0.1504267	0.0636568
O	-2.3494184	-0.3334891	-0.3934546
H	-2.4981695	-0.9184899	-1.1535847
H	-2.5669081	0.5941460	-0.7181396
O	-0.0770032	2.6939015	-0.4851047
H	0.5695987	2.8751284	-1.1858779
H	0.1368667	1.7690870	-0.1493959
O	-2.6089067	2.2068677	-1.2060956
H	-3.1871564	2.7720598	-0.6689070
H	-1.6704720	2.5002931	-0.9903299

(O2-)(H2O)4

14

O	-2.0348679	1.2962839	0.0586634
O	-0.7365408	1.4891336	0.3410885
O	0.1418729	-1.0738342	1.2573962
H	0.0073547	-0.1341446	0.9750306
H	-0.7833203	-1.3996099	1.2130650
O	-2.6651567	-1.2812017	0.4508947
H	-2.4019274	-1.6381608	-0.4130831
H	-2.4659828	-0.2888514	0.3512277
O	0.0031780	3.9493670	-0.4238243
H	0.3272724	3.7474333	-1.3167213
H	-0.2722463	3.0348321	-0.0736065
O	-2.8213129	3.7617291	-1.1682811
H	-2.7251494	2.8602830	-0.7704853
H	-1.9484439	4.1459018	-0.9338914

(OH)(H2O)4

14

O	-0.5394743	-1.2592894	0.2790870
H	-0.6376506	-0.2351106	0.2771751
O	-0.8265206	1.3307387	0.4718298
H	-0.3973090	1.6881990	1.3182805
H	-1.7353613	1.6706072	0.4607562
O	0.3265628	2.2069776	2.6736535
H	0.6303842	1.4192540	3.2263534
H	1.1293747	2.7150083	2.4750945
O	1.0723858	0.0360200	4.0249582
H	1.1384191	-0.7269067	3.3718704
H	1.9185873	0.0504360	4.4992766
O	1.2230378	-1.8960066	2.1895905
H	0.9949424	-2.8018834	2.4535409
H	0.5998867	-1.6734574	1.4299538

(OOH)(H2O)4

15

O	-1.9776665	1.1748431	0.0276327
H	-2.3554608	2.0851302	-0.3744648
O	-0.6677277	1.1758094	-0.2391729
O	0.2460172	-1.2313888	1.4289590
H	-0.6679444	-1.5865682	1.4127848
H	0.1921905	-0.4814134	0.8081329
O	-2.6830389	-1.4569658	1.3108353
H	-2.9318334	-1.2974809	2.2364788
H	-2.6287806	-0.5659036	0.9129064
O	-0.1430759	3.6116949	-1.5261793
H	0.4787894	4.1903381	-1.0550666
H	-0.0727363	2.7200675	-1.0968960
O	-2.6855320	3.4169572	-0.9291595
H	-1.7713813	3.7223329	-1.2324444
H	-3.2560948	3.4093879	-1.7156834

(OOH+)(H2O)4

15

O	-2.1761066	1.2972325	-0.3096132
H	-2.2086647	2.7831071	-0.9457842
O	-1.1070587	0.6981643	-0.4742169
O	-0.5485890	-0.9379725	1.3601093
H	-1.3224225	-1.4731855	1.6822900
H	-0.0143989	-1.5659068	0.8428137
O	-2.6486129	-2.5018679	2.2683799
H	-2.4052480	-3.2593191	2.8276206
H	-3.4113124	-2.0932838	2.7111154
O	0.0086998	4.6886395	-1.8104146
H	0.2963262	5.4378335	-1.2566369
H	0.7893288	4.1402986	-2.0096913
O	-2.1914444	3.7337027	-1.3137653
H	-1.1777696	4.1215240	-1.5355644
H	-2.8070027	3.8178739	-2.0679790

(H2O)4

12

O	1.8922773	0.0003700	-0.0287481
O	-1.8922675	-0.0003681	-0.0287572
O	0.0003696	-1.8922752	0.0287497
O	-0.0003685	1.8922702	0.0287549
H	1.2721418	-0.7927643	-0.0243494
H	-1.2721454	0.7927608	-0.0243491
H	-0.7927637	-1.2721424	0.0243495
H	0.7927618	1.2721446	0.0243490
H	2.4494373	-0.1002151	0.7595129
H	-2.4494435	0.1002160	0.7595217
H	-0.1002152	-2.4494384	-0.7595144
H	0.1002160	2.4494420	-0.7595195

S7 Supplementary references (cited in main text)

[51] Pronk, S. *et al.* GROMACS 4.5: a high-throughput and highly parallel open source molecular simulation toolkit. *Bioinformatics* **29**, 845–854 (2013).

[52] Best, R. B. & Mittal, J. Protein simulations with an optimized water model: cooperative helix formation and temperature-induced unfolded state collapse. *J. Phys. Chem. B.* **114**, 14916–14923 (2010).

[53] Abascal, J. L. F. & Vega, C. A general purpose model for the condensed phases of water: TIP4P/2005. *J. Chem. Phys.* **123**, 234505–234512 (2005).

[54] Chang, C. H. & Kim, K. Density functional theory calculation of bonding and charge parameters for molecular dynamics studies on [FeFe] hydrogenases. *J. Chem. Theory Comput.* **5**, 1137–1145 (2009).

[55] Dudko, O. K.; Hummer, G. & Szabo, A. Intrinsic rates and activation free energies from single-molecule pulling experiments. *Phys. Rev. Lett.* **96**, 108101–108104 (2006).

[56] Berezhkovskii, A., Hummer, G. & Szabo, A. Reactive flux and folding pathways in network models of coarse-grained protein dynamics. *J. Chem. Phys.* **130**, 205102–205105 (2009).

[57] Liu, C., Liu, T. & Hall, M. B. Influence of the density functional and basis set on the relative stabilities of oxygenated isomers of diiron models for the active site of [FeFe]-hydrogenase. *J. Chem. Theory Comput.* **11**, 205–214 (2015).

[58] Fourmond, V. QSoas: a versatile software for data analysis. *Anal. Chem.* **88**, 5050–5052 (2016).

References

(1) Wang, P.-h.; Bruschi, M.; De Gioia, L.; Blumberger, J. *J. Am. Chem. Soc.* **2013**, *135*, 9493–9502.

(2) Wang, P.-h.; Best, R. B.; Blumberger, J. *J. Am. Chem. Soc.* **2011**, *133*, 3548–3556.

(3) Wang, P.-h.; Best, R. B.; Blumberger, J. *Phys. Chem. Chem. Phys.* **2011**, *13*, 7708–7719.

(4) Wang, P.-h.; Blumberger, J. *Proc. Natl. Acad. Sci. U.S.A.* **2012**, *109*, 6399–6404.

(5) De Sancho, D.; Kubas, A.; Wang, P.-H.; Blumberger, J.; Best, R. B. *J. Chem. Theory Comput.* **2015**, *11*, 1919–1927.

(6) Mulder, D. W.; Boyd, E. S.; Sarma, R.; Lange, R. K.; Endrizzi, J. A.; Broderick, J. B.; Peters, J. W. *Nature* **2010**, *465*, 248–251.

(7) Pandey, A. S.; Harris, T. V.; Giles, L. J.; Peters, J. W.; Szilagyi, R. K. *J. Am. Chem. Soc.* **2008**, *130*, 4533–4540.

(8) Thompson, J. D.; Higgins, D. G.; Gibson, T. J. *Nucleic Acids Research* **1994**, *22*, 4673–4680.

(9) Roberts, E.; Eargle, J.; Wright, D.; Luthey-Schulten, Z. *BMC Bioinformatics* **2006**, *7*, 1–11.

(10) Humphrey, W.; Dalke, A.; Schulten, K. *Journal of Molecular Graphics* **1996**, *14*, 33 – 38.

(11) Pronk, S.; Páll, S.; Schulz, R.; Larsson, P.; Bjelkmar, P.; Apostolov, R.; Shirts, M. R.; Smith, J. C.; Kasson, P. M.; van der Spoel, D.; Hess, B.; Lindahl, E. *Bioinformatics* **2013**, *29*, 845–854.

(12) Best, R. B.; Mittal, J. *J. Phys. Chem. B.* **2010**, *114*, 14916–14923.

(13) Abascal, J. L. F.; Vega, C. *J. Chem. Phys.* **2005**, *123*, 234505.

(14) Chang, C. H.; Kim, K. *J. Chem. Theory Comput.* **2009**, *5*, 1137–1145.

(15) Bouanich, J.-P. *J. Quant. Spectrosc. Radiat. Transf.* **1992**, *47*, 243 – 250.

(16) Buckingham, A. D.; Disch, R. L.; Dunmur, D. A. *J. Am. Chem. Soc.* **1968**, *90*, 3104–3107.

(17) Darden, T.; York, D.; Pedersen, L. *J. Chem. Phys.* **1993**, *98*, 10089–10092.

(18) Singhal, N.; Pande, V. S. *J. Chem. Phys.* **2005**, *123*, 204909.

(19) Dudko, O. K.; Hummer, G.; Szabo, A. *Phys. Rev. Lett.* **2006**, *96*, 108101–108104.

(20) Chodera, J. D.; Singhal, N.; Pande, V. S.; Dill, K. A.; Swope, W. C. *J. Chem. Phys.* **2007**, *126*, 155101.

(21) Noe, F.; Horenko, I.; Schutte, C.; Smith, J. C. *J. Chem. Phys.* **2007**, *126*, 155102.

(22) Buchete, N.-V.; Hummer, G. *J. Phys. Chem. B* **2008**, *112*, 6057–6069.

(23) Daura, X.; Gademann, K.; Jaun, B.; Seebach, D.; van Gunsteren, W. F.; Mark, A. E. *Angew. Chem. Int. Ed.* **1999**, *38*, 236–240.

(24) Schutte, C.; Noe, F.; Lu, J.; Sarich, M.; Vanden-Eijnden, E. *J. Chem. Phys.* **2011**, *134*, 204105.

(25) Prinz, J.-H.; Wu, H.; Sarich, M.; Keller, B.; Senne, M.; Held, M.; Chodera, J. D.; Schutte, C.; Noe, F. *J. Chem. Phys.* **2011**, *134*, 174105.

(26) De Sancho, D.; Mittal, J.; Best, R. B. *J. Chem. Theory Comput.* **2013**, *9*, 1743–1753.

(27) Greco, C.; Fourmond, V.; Baffert, C.; Wang, P.-h.; Dementin, S.; Bertrand, P.; Bruschi, M.; Blumberger, J.; de Gioia, L.; Leger, C. *Energy & Environ. Sci.* **2014**, *7*, 3543–3573.

(28) Cornish, A. J.; Gärtner, K.; Yang, H.; Peters, J. W.; Hegg, E. L. *J. Biol. Chem.* **2011**, *286*, 38341–7.

(29) Knörzer, P.; Silakov, A.; Foster, C. E.; Armstrong, F. A.; Lubitz, W.; Happe, T. *J. Biol. Chem.* **2012**, *287*, 1489–99.

(30) Hong, G.; Cornish, A. J.; Hegg, E. L.; Pachter, R. *Biochim. Biophys. Acta* **2011**, *1807*, 510–7.

(31) Long, H.; King, P. W.; Chang, C. H. *J. Phys. Chem. B* **2014**, *118*, 890–900.

(32) Kubas, A.; Sancho, D. D.; Best, R.; Blumberger, J. *Angew. Chem. Int. Ed.* **2014**, *53*, 4081–4084.

(33) Stiebritz, M. T.; Reiher, M. *Inorganic chemistry* **2009**, *48*, 7127–7140.

(34) Bruska, M. K.; Stiebritz, M. T.; Reiher, M. *J. Am. Chem. Soc.* **2011**, *133*, 20588–20603.

(35) Yamaguchi, K. *Chem. Phys. Lett.* **1975**, *33*, 330–335.

(36) Noodleman, L. *J. Chem. Phys.* **1981**, *74*, 5737–5743.

(37) Dirac, P. **1929**, *123*, 714–733.

(38) Slater, J. C. *Phys. Rev.* **1951**, *81*, 385–390.

(39) Perdew, J. *Phys. Rev. B* **1986**, *33*, 8822–8824.

(40) Becke, A. D. *Phys. Rev. A* **1988**, *38*, 3098–3100.

(41) Vosko, S. H.; Wilk, L.; Nusair, M. **1980**, *58*, 1200.

(42) Grimme, S.; Antony, J.; Ehrlich, S.; Krieg, H. *J. Chem. Phys.* **2010**, *132*, 154104–154119.

(43) Grimme, S.; Ehrlich, S.; Goerigk, L. *J. Chem. Phys.* **2011**, *32*, 1456–1465.

(44) Weigend, F.; Häser, M.; Patzelt, H.; Ahlrichs, R. *Chem. Phys. Lett.* **1998**, *294*, 143–152.

(45) Weigend, F.; Ahlrichs, R. **2005**, *7*, 3297–305.

(46) Eichkorn, K.; Treutler, O.; Öhm, H.; Häser, M.; Ahlrichs, R. *Chem. Phys. Lett.* **1995**, *240*, 283–290.

(47) Sierka, M.; Hogekamp, A.; Ahlrichs, R. *J. Chem. Phys.* **2003**, *118*, 9136.

(48) Weigend, F. *Phys. Chem. Chem. Phys.* **2006**, *8*, 1057–65.

(49) Lee, C.; Yang, W.; Parr, R. G. *Phys. Rev. B* **1988**, *37*, 785–789.

(50) Becke, A. D. *J. Chem. Phys.* **1993**, *98*, 5648–5652.

(51) Klamt, A.; Schuurmann, G. *J. Chem. Soc., Perkin Trans. 2* **1993**, 799–805.

(52) TURBOMOLE V6.3 2010, a development of University of Karlsruhe and Forschungszentrum Karlsruhe GmbH, 1989-2007, TURBOMOLE GmbH, since 2007; available from `http://www.turbomole.com`.

(53) Reed, A. E.; Weinstock, R. B.; Weinhold, F. *J. Chem. Phys.* **1985**, *83*.

(54) Tao, J.; Perdew, J. P.; Staroverov, V. N.; Scuseria, G. E. *Phys. Rev. Lett.* **2003**, *91*, 146401.

(55) Perdew, J. P.; Ernzerhof, M.; Burke, K. *J. Chem. Phys.* **1996**, *105*.

(56) Adamo, C.; Barone, V. *J. Chem. Phys.* **1999**, *110*.

(57) Yanai, T.; Tew, D. P.; Handy, N. C. *Chem. Phys. Lett.* **2004**, *393*, 51–57.

(58) Huntington, L. M. J.; Nooijen, M. *J. Chem. Phys.* **2010**, *133*, 184109.

(59) Riplinger, C.; Neese, F. *J. Chem. Phys.* **2013**, *138*, 34106.

(60) Huntington, L. M. J.; Hansen, A.; Neese, F.; Nooijen, M. *J. Chem. Phys.* **2012**, *136*, 64101.

(61) Neese, F. *Wiley Interdisciplinary Reviews: Computational Molecular Science* **2012**, *2*, 73–78.

(62) Rienstra-Kiracofe, J. C.; Allen, W. D.; ; III, H. F. S. *The Journal of Physical Chemistry A* **2000**, *104*, 9823–9840.

(63) Jaque, P.; Marenich, A. V.; Cramer, C. J.; Truhlar, D. G. *The Journal of Physical Chemistry C* **2007**, *111*, 5783–5799.

(64) Kelly, C. P.; Cramer, C. J.; Truhlar, D. G. *The Journal of Physical Chemistry A* **2006**, *110*, 2493–2499, PMID: 16480309.

(65) Bielski, B. H. J.; Cabelli, D. E.; Arudi, R. L.; Ross, A. B. *J. Phys. Chem. Ref. Data* **1985**, *14*, 1041–1100.

(66) Wood, P. *Biochemical Journal* **1988**, *253*, 287–289.

(67) Silakov, A.; Kamp, C.; Reijerse, E.; Happe, T.; Lubitz, W. *Biochemistry* **2009**, *48*, 7780–7786.

(68) Liptak, M. D.; Shields, G. C. *International Journal of Quantum Chemistry* **2001**, *85*, 727–741.

(69) Palascak, M. W.; ; Shields*, G. C. *The Journal of Physical Chemistry A* **2004**, *108*, 3692–3694.

(70) Sybirna, K.; Antoine, T.; Lindberg, P.; Fourmond, V.; Rousset, M.; Méjean, V.; Bottin, H. *BMC biotech.* **2008**, *8*, 73+.

(71) Orain, C.; Saujet, L.; Gauquelin, C.; Soucaille, P.; Meynial-Salles, I.; Baffert, C.; Fourmond, V.; Bottin, H.; Léger, C. *Journal of the American Chemical Society* **2015**, *137*, 12580–12587.

(72) Fourmond, V.; Greco, C.; Sybirna, K.; Baffert, C.; Wang, P.-H. H.; Ezanno, P.; Montefiori, M.; Bruschi, M.; Meynial-Salles, I.; Soucaille, P.; Blumberger, J.; Bottin, H.; De Gioia, L.; Léger, C. *Nat. Chem.* **2014**, *6*, 336–342.